Aus dem Institut für Anatomie und Zellbiologie
(Direktor Univ.- Prof. Dr. med. Karlhans Endlich)
der Universitätsmedizin der Universität Greifswald

Thema:

Study of the effect of the podocyte-specific palladin knockout in mice with a 129 genetic background

Inaugural - Dissertation

zur

Erlangung des akademischen

Grades

Doktor der Medizin
(Dr. med.)

der

Universitätsmedizin

der

Universität Greifswald

2023

vorgelegt von:
Alina Margarethe Ritter
geb. am: 19.08.1995
in: Heilbronn

Dekan: Prof. Dr. med. Karlhans Endlich

1. Gutachterin: Prof. Dr. rer. nat. Nicole Endlich

2. Gutachterin: Prof. Dr. med. Miriam Banas

Ort, Raum: Greifswald, Klinik für Innere Medizin A, Seminarraum (7.0.15/17)

Tag der Disputation: 22.01.2024

Preface

This cumulative dissertation is based on the articles:

Artelt N, Siegerist F, **Ritter AM**, Grisk O, Schlüter R, Endlich K, Endlich N. Comparative Analysis of Podocyte Foot Process Morphology in Three Species by 3D Super-Resolution Microscopy. Front Med (Lausanne). 2018 Oct 30;5:292. doi: 10.3389/fmed.2018.00292.

Artelt N, **Ritter AM**, Leitermann L, Kliewe F, Schlüter R, Simm S, van den Brandt J, Endlich K, Endlich N. The podocyte-specific knockout of palladin in mice with a 129 genetic background affects podocyte morphology and the expression of palladin interacting proteins. PLoS One. 2021 Dec 8;16(12):e0260878. doi: 10.1371/journal.pone.0260878.

The articles can be found in the appendix of this work. The article published in *Frontiers in Medicine* underlies the copyright regulations of the publisher Frontiers Media S.A.. The article published in *PLOS ONE* underlies the copyright regulations of the publisher Public Library of Science.

Table of content

List of figures

1. Introduction

Chronic kidney disease (CKD) is one of the world's leading public health problems, but it is often under-recognized by clinicians and patients. In 2017, it was ranked as the 12th leading cause of death and 1.2 million people died from CKD worldwide [1]. The major causes leading to CKD are diabetes, hypertension, obesity, aging and glomerulonephritis [1–3]. All of these conditions effect the filtration units of the kidney, the glomeruli. An early identification of glomerular dysfunction is needed to prevent disease progression and associated morbidity and mortality.

Glomeruli consist of a capillary network supported by a scaffold of mesangial cells. The double-walled Bowman´s capsule surrounds the glomerulus and is lined by parietal epithelial cells (PECs). Highly specialized postmitotic visceral epithelial cells of the glomerulus, the podocytes, are attached to the outside of the capillary loops. Podocytes form primary processes from which secondary foot processes originate. These foot processes interdigitate with the foot processes of the neighbouring cell (Figure 1B) and lead to an almost complete coverage of the glomerular basement membrane (GBM) to which the podocyte adheres. The glomerular basement membrane lies between the fenestrated capillary endothelium and the podocytes. Together they form the glomerular filtration barrier (Figure 1A). Main function is the proper filtration of molecular components from the blood according to size, shape and charge.

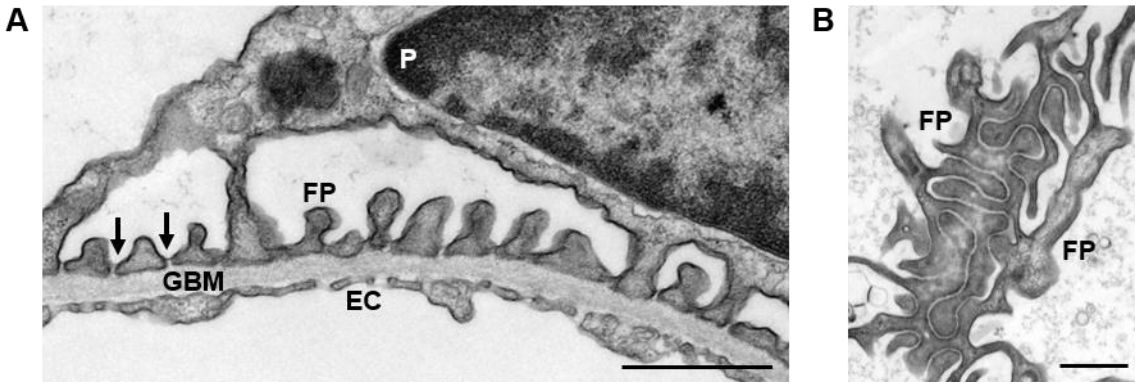

Figure 1: Murine structure of the glomerular filtration barrier. (A) Transmission electron microscopy image of the glomerular filtration barrier consisting of podocyte foot processes (FP), glomerular basement membrane (GBM) and endothelial cells (EC). Arrows mark the slit diaphragm between neighboring foot processes. P stands for podocyte. (B) TEM image of interdigitating foot processes (FP) of neighboring podocytes. Scale bars represents 1 µm.

Between interdigitating foot processes only narrow filtration slits, which are bridged by a so-called slit diaphragm, remain (Figure 1A, B). The slit diaphragm plays a key role for size-selective filtration [4]. Nephrin and podocin are central molecular components of the slit diaphragm that anchor the cytoskeleton to the plasma membrane and form flexible, spring-like protein bridges that prevent the passage of macromolecules [5–7].

The actin cytoskeleton is the key component of the podocyte foot processes. Together with specific actin binding proteins, like the actin filament crosslinking protein α-actinin-4 it defines cell architecture and structure [8,9]. Mutations in the *ACTN4* gen or loss of the protein leads to an actin cytoskeleton remodelling and the loss of the interdigitating foot processes pattern, called foot process effacement [10–12]. Effacement leads to a reduction and breakdown of the glomerular filtration barrier function resulting in a leakage of macromolecules (proteinuria) such as albumin in focal segmental glomerulosclerosis (FSGS), minimal change disease, and diabetes, among others [9,13]. In conclusion, proteins involved in actin filament reorganization are important for podocyte morphology and thus normal kidney function.

Palladin, a novel actin-associated phosphoprotein was first described in 2000 by Parast and Otey et al. [14]. In rat choriocarcinoma cells the palladin expression increased, when they began to assemble stress fibers [14]. Furthermore, the reduction of palladin expression in fibroblasts resulted in a complete loss of actin stress fibers and focal adhesions, leading to rounding cells [14]. In injured astrocytes and COS-7 cells (african green monkey kidney fibroblast-like cells) the overexpression of palladin induced formation of robust actin bundles [15,16]. Through its ubiquitous expression in embryonic tissues the palladin knockout in mice leads to defects of cranial neural tube closure and embryonic lethality around E15.5 [17,18]. These results show that palladin has a crucial influence on normal actin cytoskeleton organization, focal adhesions and plays an important role as cytoskeletal scaffold.

Different palladin isoforms are generated by alternative splicing and expressed in a tissue- and development-specific manner [14,19,20]. These isoforms consist of immunoglobulin domains and proline-rich regions. Through these palladin may not only affect actin

organization directly via a specific binding site for F-actin [21,22], but also indirectly via interaction with actin-associated proteins. The LIM and SH3 protein 1 (Lasp-1) directly binds to palladin and is known to play an important role in actin cytoskeleton organization and cell motility [19,23,24]. Furthermore, the actin binding protein α-actinin-1 [16], ezrin [25], and the vasodilator-stimulated phosphoprotein (VASP), which regulates actin polymerization, bind to palladin [26]. Ezrin belongs to the ezrin/radixin/moesin protein family, that are direct or indirect cross-linkers between plasma membrane proteins and the cytoskeleton [27]. Pdlim2, another palladin binding proteins regulates actin dynamics in podocyte foot processes [28,29]. In patients with minimal change nephrotic syndrome and membranous nephropathy a reduced expression of Pdlim2 in podocytes was found. Moreover, Pdlim2 interacts with two regulators of actin assembly, α-actinin-4 and angiomotin-like 1 (Amotl1) [29]. In addition, the anti-aging protein Klotho seems to promote the expression of Pdlim2 protein and Pdlim2 transcription level and regulate renal inflammation through pdlim2/NF- kB p65 pathway [30].

Our group showed that palladin is highly expressed in the kidney. Especially podocytes exhibit a strong signal for palladin *in vivo* and *in vitro* [31]. Studying the role of palladin in the morphology and stability of the actin cytoskeleton our group revealed that cultured palladin-knockdown (PalldKD) podocytes developed fewer actin-filaments and a higher number of small focal adhesions [32]. The expression of synaptopodin and α-actinin-4 was significantly reduced in these PalldKD podocytes. Moreover, treating PalldKD podocytes with inhibitors of actin polymerization revealed an induced disassembly of the actin filaments compared to the controls [32]. Additionally, our group showed that the expression of palladin is downregulated in patients suffering from diabetic nephropathy and FSGS [32]. However, the importance of palladin for renal function as well as for the podocytes could not be clarified, since the ubiquitous knockout is intrauterine lethal in mice. Therefore, our group generated a podocyte-specific knockout for palladin in C57BL/6 mice (PodoPalldBL/6-/-). PodoPalldBL/6-/- mice 6 months of age developed glomeruli with a disturbed morphology. Dilatation of the capillary tuft as well as a mild podocyte foot process effacement with a reduced nephrin expression could be shown [32].

Many studies showed that mice with a C57BL/6 genetic background are relatively more resistant against kidney damage than mice with a 129 genetic background. Mice with 129 genetic background seem to be more susceptible to glomerulosclerosis, proteinuria, the inducement of chronic kidney disease and other certain renal models [33–36]. Taken together, this indicates the important role for the genetic background in which animal models are generated. For that reason, we wanted to study the effect of the podocyte-specific palladin knockout in mice with the more sensitive 129 genetic background (PodoPalld129-/-).

Aim of the present work

The aim of the present work was to investigate the influence of the actin-associated protein palladin on podocytes and thus glomerular function and morphology in 6- and 12-month old PodoPalld129-/- mice.

First of all, we backcrossed the PodoPalldBL/6-/- mice with the 129 strain to generate the PodoPalld129-/- mice. In a second step we analysed the glomerular morphology as well as the expression of palladin- and actin-binding proteins in 6 months and 12 months old mice more detailed. Moreover, we had a closer look on the glomerular filtration barrier and, consequently, the urine of PodoPalld129-/- mice of both ages.

2. Material and Methods

2.1 PodoPalld129-/- mice strain

Detailed information about the generation of the podocyte-specific palladin knockout mice with a 129 genetic background (PodoPalld129-/-) is provided in the *PLOS ONE* publication. In brief, PodoPalldBL/6-/- mice having a C57BL/6 genetic background were generated using the Cre/loxP system as described priorly by Artelt et al. [32]. Establishing the new mouse line these mice were backcrossed 8 times to the 129 (129S2/SvPasCrl) genetic background using the "*speed congenics*" approach [37,38]. For all experiments 6 months and 12 months old mice with heterozygous Cre-recombinase expression were used as the podocyte-specific palladin knockout mice (PodoPalld129-/-) and mice without Cre-recombinase expression were used as controls (PodoPalld129+/+) [38] (Figure 2).

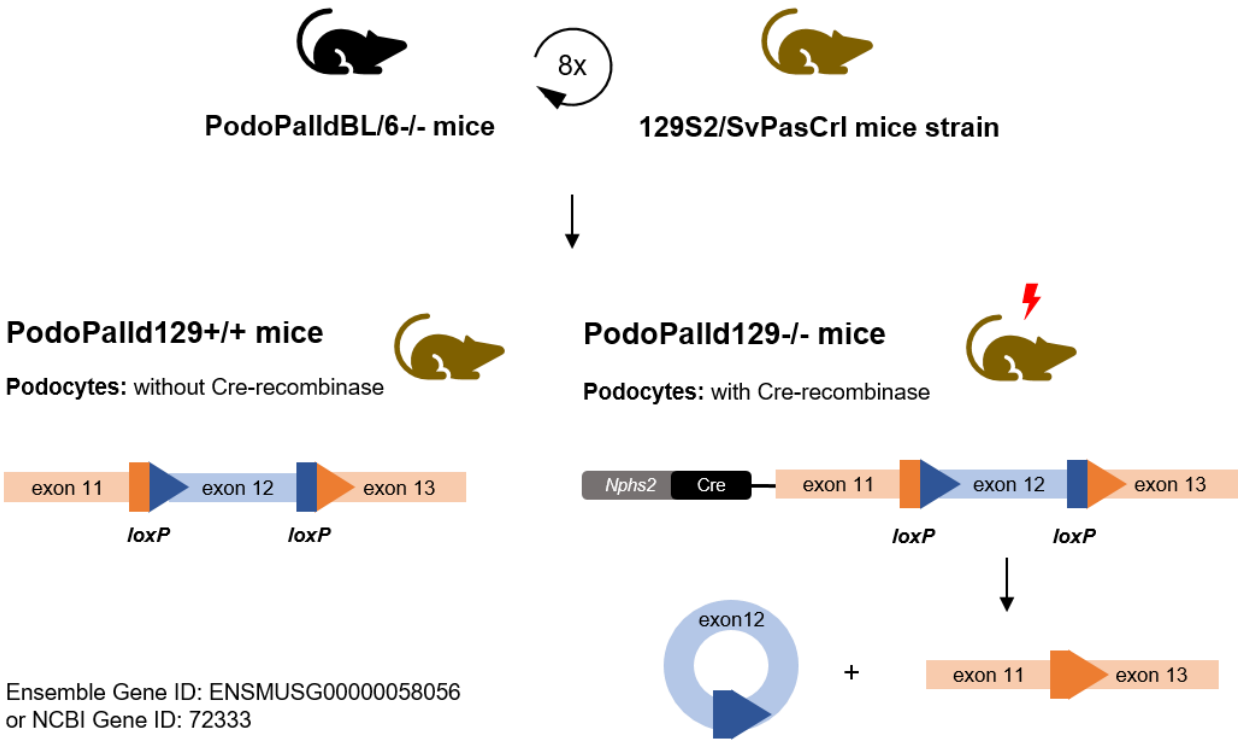

Figure 2: Generation of PodoPalld129-/- mice. PodoPalldBL/6-/- mice were backcrossed to the 129 background using 129S2/SvPasCrl mice. In the palladin gene of PodoPalld129 mice, exon 12 is flanked by loxP sites. To generate PodoPalld129-/- mice, mice were used that additionally express the Cre-recombinase under the Nphs2 promoter. The Cre-recombinase cut at the loxP sites flanking E12 of the palladin gene which resulted in the palladin KO specifically in podocytes. PodoPalld129+/+ mice did not express the Cre-recombinase.

Approximately 1 cm was cut from the tail tip of these mice and stored at -20°C. Later, this was used to characterize these mice [38].

2.2 Histology

Histological processing of kidney sections is described in the underlying publications [38,39]. In summary, paraffin sections (4 µm) were stained with PAS and H&E according to standard procedures [38]. Immunohistochemistry detecting palladin in mice glomeruli and Richardson´s stained semithin sections of mouse kidneys were performed as described [38]. Masson-Goldner-trichrome staining was performed as follows: First of all, the slides were deparaffinized and rehydrated. After that the slides were incubated in Iron hematoxylin solution according to Weigert for 15 min, rinsed in Aqua dest. and incubated in running tap water. After 8 min the slides were incubated in Ponceau acid fuchsin for 4 min, given in acetic acid 1% for 30 sec and incubated in Phosphomolybdic acid Orange G for maximum 30 min. We repeated the incubation in acetic acid 1% for 30 sec. The slides were then given into Light Green Goldner III for 6 min, rinsed in acetic acid 1% for 30 sec again and incubated in running tap water for 1 min. At the end the slides were dehydrated in ascending ethanol series, cleared in xylene and mounted in Eukitt (Carl Roth, Karlsruhe, Germany). All images were obtained using an Olympus BX50 microscope.

Immunofluorescence staining for *nephrin, podocin, ezrin, p-Lasp-1, integrin α8* and *Pdlim-2* was performed using a specific primary antibody that later bound to a fluorescence-labelled secondary antibody visualizing the proteins [38,39]. For imaging a confocal laser scanning microscope (Leica SP5) and a Zeiss Elyra PS.1 system performing 3D structured illumination microscopy was used [38,39].

For transmission electron microscopy, ultrathin sections of kidneys embedded in Epon 812 were prepared and processed accordingly [38]. Images were taken with a Carl Zeiss LIBRA® 120 TEM [38].

2.3 Analysis of glomerular morphology

Richardson's stained semithin sections of mouse kidneys were used to characterize glomerular abnormalities as described in the *PLOS ONE* publication [38].

In addition, the images were used to quantitatively calculate the ratio of the mesangial area per glomerular area to show mesangial changes. These morphometric measurements were made with the ImageJ-based open source software package FIJI [40]. At least n=3 mice of each group with a total of more than 30 glomeruli were analysed. Using TEM images we quantitatively analysed the contacts between podocytes and parietal epithelial cells (PEC) in the glomeruli of PodoPalld129 mice. Three animals of each group with at least 13 glomeruli were calculated. Using GraphPad Prism 9, two-way ANOVA with FDR correction was performed for statistical analysis. Statistically significant differences (p<0.05) were symbolized by an asterisk.

Analysis of the filtration slit density (FSD) were performed using the *Podocyte Exact Morphology Measurement Procedure* (PEMP) of 3D-SIM images as described detailed in the underlying article [39]. To support the obtained results, we analysed the with the FSD inversely correlated foot process area per glomerular area using the previously generated values [38].

2.4 Urine data

We collected equal volume of urine from 6 months and 12 months old PodoPalld129 mice using a sterile needle. The urinary protein concertation was measured using dip stick (Combur^{10} Test® strip, Roche). Furthermore, the urine was separated by SDS electrophoresis and stained using CBB (Coomassie Brilliant Blue). Later all the urine samples were used for detailed proteome analysis by LC-MS/MS (in cooperation with the Department of Functional Genomics Greifswald).

2.5 qRT-PCR analysis

As described detailed in the *PLOS ONE* publication RNA was extracted from isolated glomeruli and used for quantitative real-time PCR (qRT-PCR) [38].

3. Results

3.1 Podocyte-specific palladin knockout in PodoPalld129-/- mice

Since the palladin knockout in mice is lethal [17] and the effect of a knockout depends on the genetic background we backcrossed the previously described PodoPalldBL/6-/- mice [32] with the more susceptible 129 strain. The podocyte-specific palladin knockout in 6 and 12 months old mice with a 129 genetic background was confirmed on both RNA and protein levels (Figure 3) [38].

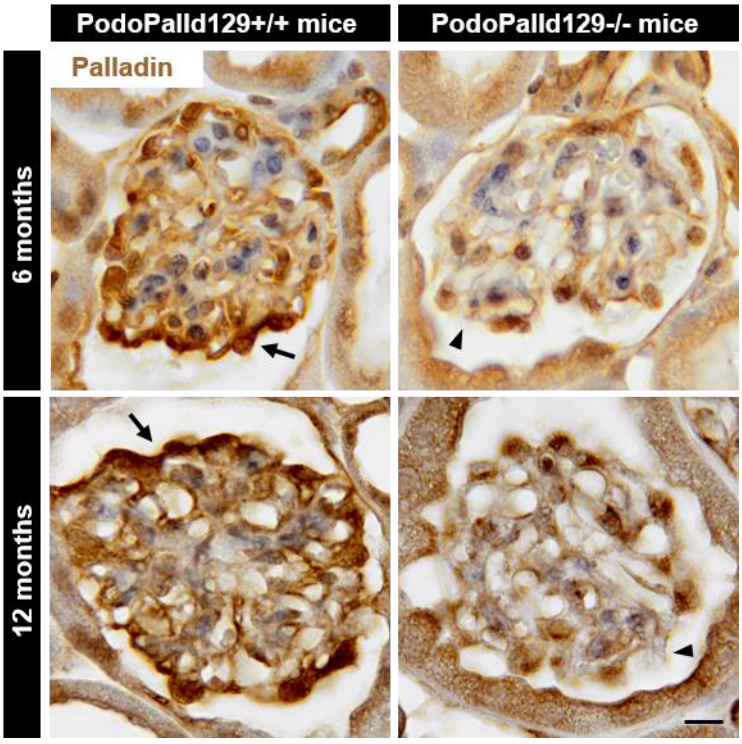

Figure 3: Confirmation of palladin KO. Immunhistochemistry staining of paraffin kidney sections confirmed the podocyte specific palladin KO in PodoPalld129-/- mice 6 months and 12 months of age. The arrows show the strong palladin expression in podocytes of PodoPalld129+/+ mice and the arrowheads the missing signal for palladin in podocytes of PodoPalld129-/- mice. Scale bar represents 10 µm. Figure modified from Artelt, Ritter et al. 2021 [38].

3.2 Analysis of the glomerular capillary tuft and mesangium

It was shown that palladin plays an important role for podocyte and glomerular morphology *in vitro* and in PodoPalldBL/6-/- mice [32]. To study the glomerular morphology in detail, we performed histological and ultrastructural analysis of 6 month and 12 months old PodoPalld129 mice. PodoPalld129-/- mice of both age groups stained

with Masson-Goldner-trichrome (MGT; Figure 4A), Periodic Acid Schiff (PAS) and Hematoxylin and Eosin (H&E), which showed a marked dilatation of the glomerular capillaries [38]. This finding was verified by quantitative analysis of the capillary area per glomerular area, supporting that glomeruli of 6 months and 12 months old PodoPalld129-/- mice have significantly enlarged capillaries compared to the control glomeruli [38]. According to these findings, we examined the mesangium since it is known that a dilatation of the capillary tuft could be caused by a reduction of the glomerular mesangium. Quantitative analysis of the mesangial area per glomerular area revealed that the mesangium of PodoPalld129-/- mice was significantly reduced (6 months: 0.54±0.06, $p<0.05$; 12 months: 0.50±0.07, $p<0.05$; mean±SD) in comparison to the control mice (6 months: 0.64±0.03, 12 months: 0.60±0.03) (n≥3 animals and >30 glomeruli per group, Figure 4B). In addition, we could show a marked reduction of the mesangial marker protein integrin α8 in immunofluorescence staining and Western blot analysis [38]. These findings let suggest that palladin might have an influence on the mesangium and capillary tuft formation.

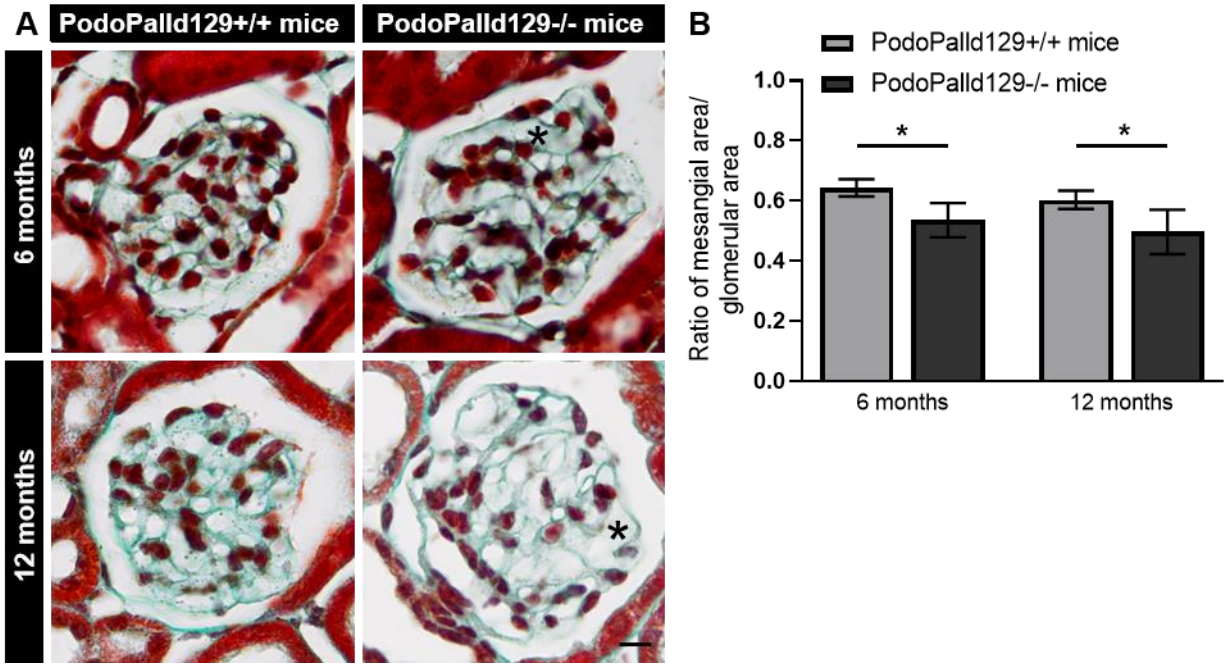

Figure 4: Glomeruli of PodoPalld129-/- mice showed dilated capillaries and reduced mesangial/glomerular area. (A) The Masson-Goldner-trichrome staining of paraffin kidney sections showed dilated capillaries in 6 and 12 months old PodoPalld129-/- mice (asterisks). Scale bar represents 10 µm. (B) Quantitative analysis of the mesangial area/glomerular area confirmed that PodoPalld129-/- mice of both age groups have significantly more glomeruli with reduced mesangium than controls of the same age (mean±SD, *$p<0.05$; two-way ANOVA with FDR correction).

3.3 Morphological changes of podocytes in PodoPalld129-/- mice

Results of the analysis of podocyte morphology in 6 and 12 months old PodoPalld129-/- mice compared to the controls are shown in detail in the *PLOS ONE* publication. In summary, we found podocytes in both age groups of PodoPalld129-/- mice that develop significantly more morphological deviations such as an enlarged sub-podocyte space, autophagosomes and laminar bodies and significantly fewer podocytes with normal morphology than the controls [38].

In the *PLOS ONE* publication we could already show regions of podocytes that have close contact to parietal epithelial cells in 6 and 12 months old PodoPalld129-/- mice [38]. This observation was underlined by quantitative analysis of transmission electron microscopy (TEM) sections. We were able to show that podocytes of PodoPalld129-/- mice have significantly more contacts to parietal epithelial cells (6 months: 2.19±0.89, $p<0.05$; 12 months: 0.83±0.76, ns; mean±SD) than the controls (6 months: 0.75±0.29, 12 months: 0.32±0.16; mean±SD) (n≥3 animals and >3 glomeruli per group, Figure 5B). Moreover, we found podocytes with broadened primary processes in 6 months and 12 months old PodoPalld129-/- mice (Figure 5A).

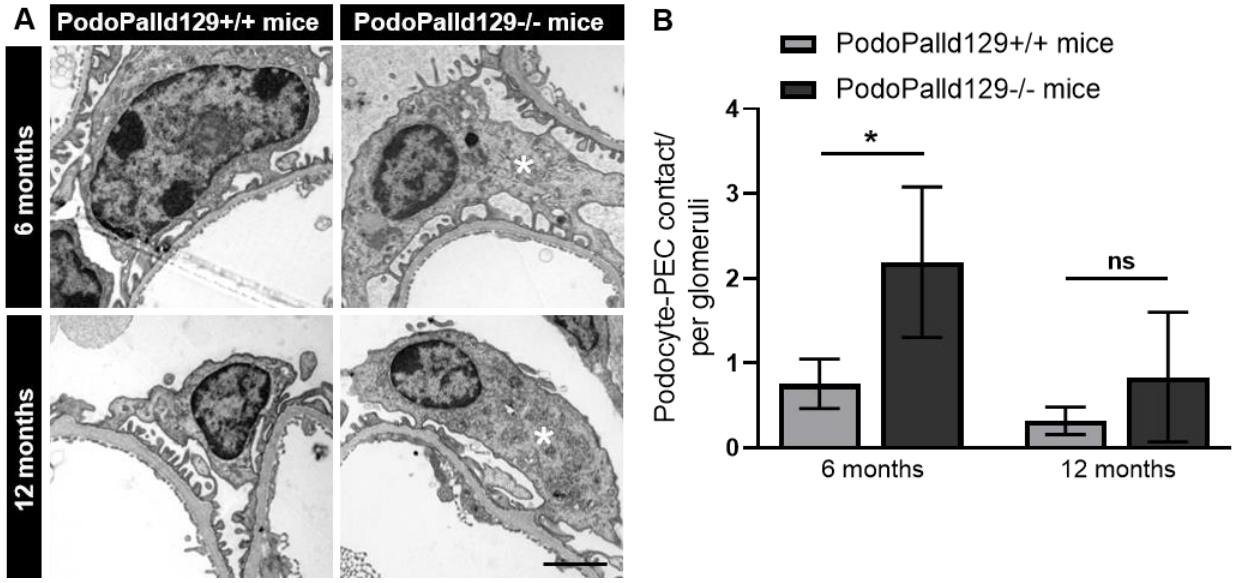

Figure 5: Podocytes show morphological alterations in PodoPalld129-/- mice. (A) TEM images show podocytes with (asterisk) and thickened primary processes (asterisk) in 6 and 12 months old PodoPalld129-/- mice. Scale bar represents 2 µm. (B) Quantitative analysis confirmed that PodoPalld129-/- mice 6 months of age had significantly more contacts between podocytes and PECs than controls of the same age. 12 months old PodoPalld129-/- mice showed no significant increase compared to the controls (mean±SD, *p<0.05, ns, not significant; two-way ANOVA with FDR correction).

3.4 Glomerular filtration barrier in PodoPalld129-/- mice

Because PodoPalld129-/- mice evolved podocytes with morphological alterations we had a closer look on the glomerular filtration barrier, especially on the glomerular basement membrane (GBM) and podocyte foot processes. In transmission electron microscopy of 6 and 12 months old PodoPalld129-/- mice we observed glomeruli with a partially thickened glomerular basement membrane. Nevertheless, we found this observation increasingly in 12 months old PodoPalld129-/- mice (Figure 6B).

To analyse the slit diaphragm, we performed immunofluorescence stainings. The expression of the slit diaphragm proteins nephrin (Figure 6A) and podocin was reduced in 6 and 12 months old PodoPalld129-/- mice compared to the controls [38]. Interestingly, the mRNA expressions of these proteins showed no significant reduction [38]. In TEM and scanning electron microscopy (SEM) analysis, we observed a marked effacement of the podocyte food processes corresponding to the reduced slit diaphragm proteins [38]. This observation was underlined by the published *Podocyte Exact Morphology Measurement Procedure* (*PEMP*) that quantifies podocyte foot process morphology on nephrin-stained kidney sections by measuring the filtration slit density (FSD) [39]. The FSD, which is the length of the filtration slit per marked area, is significantly lower in PodoPalld129-/- mice 6 and 12 months of age compared to the controls [39]. In accordance to that the quantification of the foot process area, which inversely correlates to the FSD verified that PodoPalld129-/- mice 12 months of age showed an increased podocyte foot process effacement compared to the PodoPalld129-/-mice 6 months of age [38]. Moreover, we observed significantly more effaced podocyte food processes in 12 months old control mice compared to their 6 months old littermates indicating that not only the genotype but also aging affects podocyte foot process morphology [38,39].

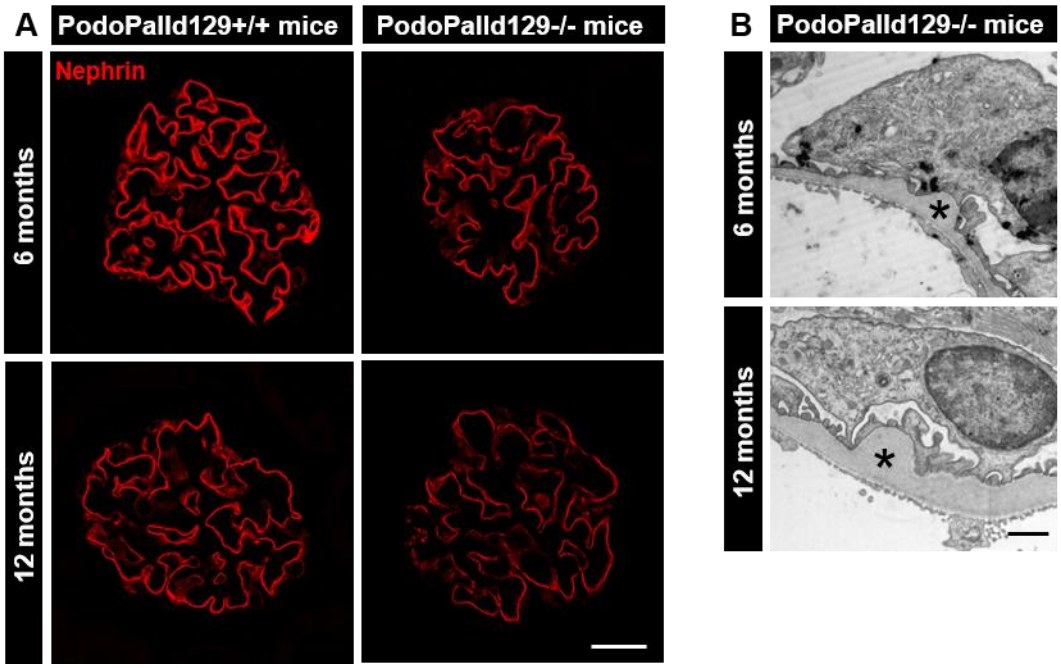

Figure 6: Morphological changes of glomerular filtration barrier components in PodoPalld129-/- mice. (A) PodoPalld129-/- mice showed a reduced expression of the slit membrane protein nephrin in immunofluorescence stainings compared with the corresponding controls. Scale bar represents 20 µm. (B) TEM illustrated a partially thickened GBM (asterisk) in PodoPalld129-/- mice. Scale bar represents 1 µm. Figure partially modified from Artelt, Ritter et al. 2021 [38].

3.5 Urine analysis in PodoPalld129-/- mice

It is known that morphological changes in the glomerular filtration barrier especially effaced podocyte foot processes are associated with the presence of proteinuria. Since PodoPalld129-/- glomeruli exhibited significantly effaced podocyte foot processes at both 6 and 12 months of age, we analysed the urine of these mice for the occurrence of proteinuria. In dip stick and SDS electrophoresis analysis, we could not detect proteinuria or albuminuria in 6 months (Figure 7A) and 12 months old PodoPalld129-/- mice [38]. Nevertheless, we analysed the urine of the animals for pathological components by proteome analysis. Although proteinuria was not detected, an increase in the urinary trefoil factor 1 (Tff1) expression was measured by LC-MS/MS in 6 (+34%) as well as 12 months old (+118%) PodoPalld129-/- mice compared with the controls (Figure 7B).

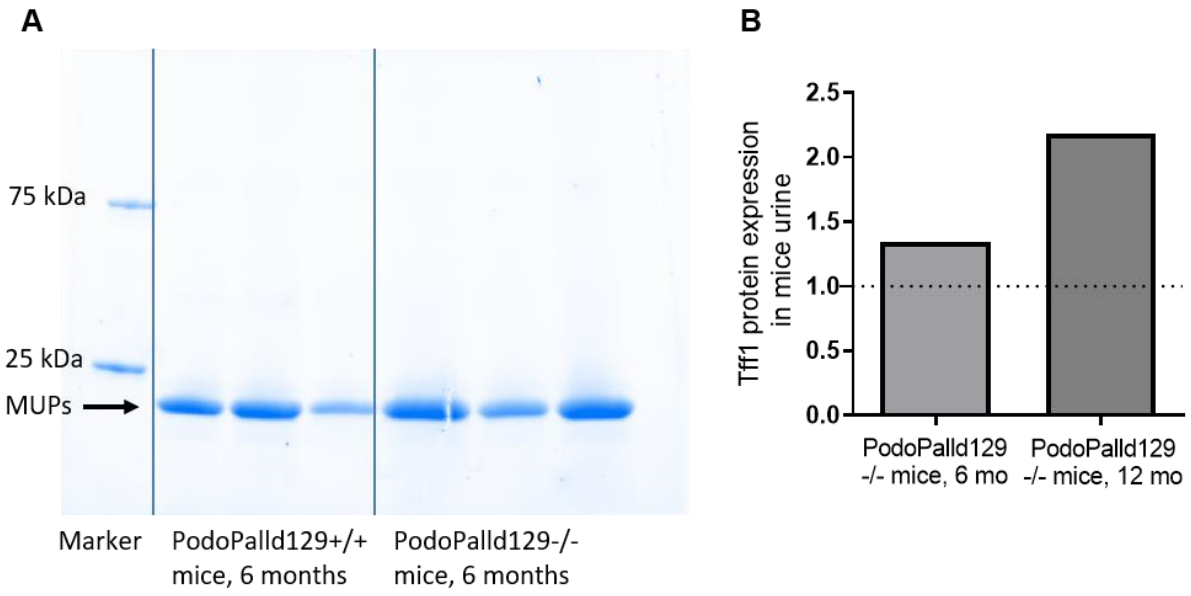

Figure 7: Urine analysis of PodoPalld129-/- mice. (A) 1 µl sterile mice urine from 6 months old PodoPalld129-/- mice and the corresponding controls were separated by gel electrophoresis and stained using CBB. No albumin band could be seen at 66 kDA molecular weight in PodoPalld129-/-mice 6 months of age. This indicates no increased albuminuria or proteinuria in the PodoPalld129-/- mice. A strong signal was shown by the major urinary proteins (MUPs). (B) We could detect an increase of trefoil factor 1 (Tff1) in 6 months and stronger in 12 months old PodoPalld129-/- mice urine compared to the corresponding controls.

3.6 Expression of palladin- and actin-binding proteins

We could already show that PodoPalld129-/- mice develop glomeruli with various morphological abnormalities. Since the actin-cytoskeleton and actin-binding proteins are highly relevant for podocyte morphology we investigate the role of palladin on the expression of essential palladin- and actin-binding and interacting proteins like Pdlim2, VASP, Lasp-1, ezrin, Amotl1 and Klotho, on protein and RNA levels. Pdlim-2 and phosphorylated LASP-1 (pLASP-1) was markedly reduced in immunofluorescence stainings of PodoPalld129-/- mice at 6 months and 12 months of age compared to the controls, whereas ezrin remained unchanged (Figure 8A) [38]. qRT-PCR and Western blot analysis of the 6 months old PodoPalld129-/- mice underlined the significant reduction of Pdlim2, while Ezrin and LASP-1 remained unchanged (Figure 8B) [38]. Furthermore, the mRNA levels showed a significant downregulation of *VASP* and upregulation of *Amotl1* in both age groups [38]. In addition, we examined the mRNA levels of *Pdlim2*, *LASP-1* and *ezrin* in 12 months old PodoPalld129-/- mice. *Pdlim2* was significantly

reduced in the glomeruli (12 months: 0.89±0.17, p<0.001; mean±SD) whereas *Lasp-1* was unchanged (12 months: 0.97±0.30; mean±SD). However, *ezrin* was slightly downregulated at the age of 12 months (0.92±0.18, p<0.05; mean±SD). The mRNA level of the anti-aging protein *Klotho* is significantly downregulated in 6 months (0.57±0.53, p<0.001; mean±SD) as well as 12 months (0.59±0.50, p<0.001; mean±SD) old PodoPalld129-/- mice (Figure 8B).

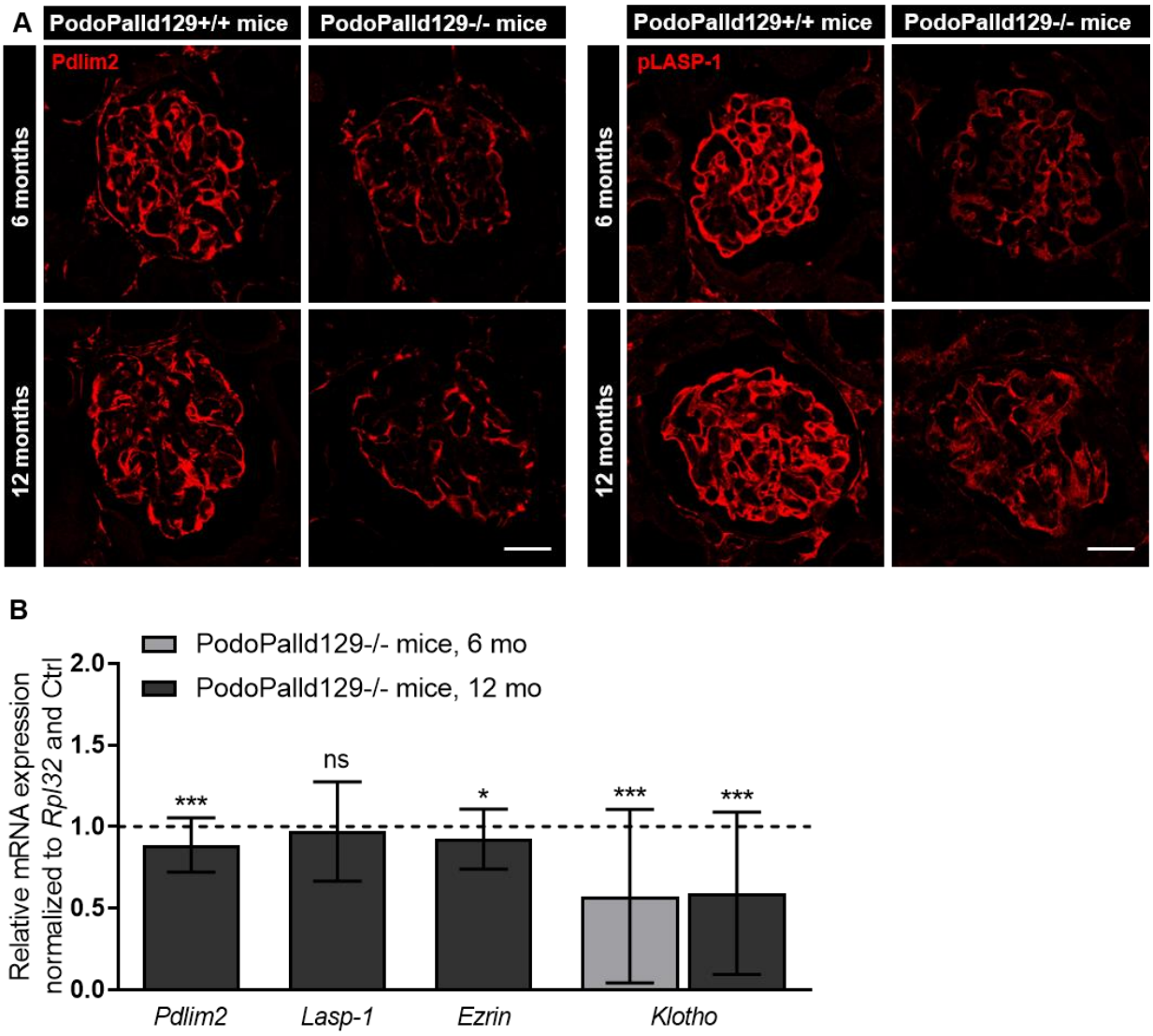

Figure 8: Protein and mRNA analysis of palladin-interacting proteins in PodoPalld129-/- mice. (A) Pdlim2 and pLasp-1 expression is reduced in immunofluorescence stainings of PodoPalld129-/- mice compared with corresponding controls. Scale bars represent 20 µm. (B) qRT-PCR analysis showed a significant downregulation of *Pdlim2* mRNA in 6 months and 12 months old PodoPalld129-/- glomeruli. There was no significant (ns) difference for the mRNA levels of *Lasp-1* (both age groups) and *ezrin* (6 months of age) in PodoPalld129-/- glomeruli compared controls, but a slightly downregulation for *ezrin* at 12 months of age (mean±SD, *p<0.05 **p<0.01 and ***p<0.001; unpaired Student's t-test). Figure partially modified from Artelt, Ritter et al. 2021 [38].

4. Discussion

The actin cytoskeleton plays a central role for the morphology of podocyte foot processes and therefore for the size-selectivity of the filtration barrier. One protein, which we have recently identified to play an essential role for the actin cytoskeleton of podocytes is palladin, a protein responsible for the crosslinking and the stabilization of actin filaments [14,21]. As shown in our recent publication, palladin knockout in PodoPalld129-/- mice resulted in disturbed podocyte morphology, foot process effacement, glomerular tuft alterations, and influenced expression of palladin- and actin-binding proteins.

Since the genetic background of a mouse strain is highly important for the severity of the induced kidney disease, we wanted to study the influence of a palladin knockout on a mouse strain described as less resistant against kidney damage, such as mice with a 129 genetic background. Thus, Hartner and colleagues have nicely shown that 129S mice treated with deoxycorticosterone acetate (DOCA) salt are more susceptible to hypertension and glomerulosclerosis associated with albuminuria than C57BL/6 mice [34]. This is in agreement with the latest finding that 129S and C57BL/6 strains have significant differences in distinct vascular properties [41]. In general, the C57BL/6 mice strain is suggested to be relatively robust against all kidney diseases. In our experiments, we further focussed on the age-related development of morphological and functional alterations in a strain-dependent way. Since it is well known that kidney functions decline with age and that there is a correlation between age and worse outcome for most glomerular diseases [42–44], we analysed 6 and 12 months old PodoPalld129-/- mice compared to the corresponding controls.

We found that PodoPalld129-/- mice showed much more glomeruli with dilated capillaries than PodoPalldBL/6-/- mice at 6 month of age [32,38]. Additionally, PodoPalld129-/- mice 6 and 12 months of age showed a significant increase of the capillary area combined with the formation of a dilated capillary tuft compared with the controls. Since mesangial cells are essential for the development and maintenance of glomerular tuft morphology [45], we studied the mesangial cells in PodoPalld129-/- mice. The PodoPalld129-/- mice showed a significant downregulation of integrin α8, a specific marker for mesangial cells

[46] indicating that a knockout of palladin in podocytes results in a loss of mesangial cells. Quantitative analysis using the ImageJ-based open source software package FIJI revealed indeed a significant reduction of the mesangial area in 6 and 12 months old PodoPalld129-/- mice compared to the controls. This finding is in agreement with previous studies of podocyte-specific VEGF-A knockdown mice that developed mesangiolysis with dilatated capillary loops [47], indicating an important crosstalk between podocytes and mesangial cells, as has been already reported for other proteins. Taken this part together, we demonstrated that palladin has an indirect effect on capillary loop formation by reducing the number of mesangial cells. Kriz previously described that these alterations may cause podocytes to be shifted radially and come into contact with parietal epithelial cells [48]. In our present study we could observe that as a consequence of capillary tuft enlargement PodoPalld129-/- mice 6 months of age developed a significant increased number of contacts between podocytes and parietal epithelial cells (PECs) compared to controls. This cellular adhesion between podocytes and PECs is the start of tuft adhesion, one of the first committed lesions for FSGS [48,49]. Despite this, 12 months old PodoPalld129-/- mice showed no significant increase in contact formations, suggesting presumed podocyte loss.

Despite glomerular tuft alterations in PodoPalld129-/- mice, we identified more podocytes with morphological abnormalities, such as an enlarged sub-podocyte space and cyst formation compared to the corresponding controls as well as to podocytes from PodoPalldBL/6-/- mice [32,38]. We believe that this is caused by the absence of the scaffolding protein palladin, which is highly important for actin cytoskeleton organisation as well as for actin polymerization and nucleation [21,32,50]. It was already shown that Rcho-1 cells collapse when palladin is absent [14]. Palladin knockout podocytes may therefore be more susceptible to mechanical stress because they cannot counteract it, as we have recently shown in living zebrafish embryos [32]. Mechanical stress might also be responsible for the thickening of the GBM that we observed in PodoPalld129-/- glomeruli 6 and 12 months of age. In a recent study we have already shown that mechanical stretched podocytes produce an increased number of extracellular matrix proteins like fibronectin [51].

Since it is well known that the morphology of podocyte foot processes is directly linked to the size selectivity of the filtration barrier, we wanted to determine whether podocyte foot processes are differentially affected by the knockout, depending on age and strain. Beside a reduced expression of the slit diaphragm proteins nephrin and podocin in PodoPalld129-/- mice, we found that 12 months old PodoPalld129-/- mice showed significantly more effaced podocyte foot processes compared to 6 months old littermates. However, this was also observed in control animals, indicating that podocyte foot process morphology changes in an age-dependent manner. Supporting this, Kos and colleagues observed in a non-quantitative manner an age-dependant increase of podocyte foot process effacement in *Actn4* deficient mice [10]. Interestingly, we found a broadening of the primary processes of podocytes in 6 and 12 months old PodoPalld129-/- mice, in contrast to controls. Kriz and colleagues hypothesized that broad and flattened primary processes are caused by retraction of the foot processes into the primary processes when the complete stage of foot process effacement is reached [13].

Although effacement is accompanied with protein leakage and albuminuria, no albuminuria was detectable in the urine of PodoPalld129-/- mice. This could be explained by an increased re-absorption of filtered albumin by the proximal tubules, as described by Dickson et al. [52]. However, we found that protein expression of Trefoil factor 1 (Tff1) was increased in the urine of PodoPalld129-/- mice, especially in mice at 12 months of age. This might be a first sign of onset of renal failure and an acute phase of kidney disease, as it was reported by Lebherz-Eichinger [53].

Since the actin cytoskeleton plays a central role for a proper 3D morphology of podocyte foot processes, we analysed palladin and actin-binding proteins such as Lasp-1 [19], Pdlim2 [28], ezrin [25] and VASP [26]. It has been reported that knockdown of palladin in HeLa cells results in loss of Lasp-1 to actin stress fibers. We hypothesized that palladin is required to recruit Lasp-1 to actin stress fibers in podocytes [19,38]. In our experiments, mRNA expression of *Lasp1* was unchanged in PodoPalld129-/- podocytes, however we observed a significant reduction of phosphorylated Lasp-1 (pLasp-1) in PodoPalld129-/- mice of both ages in contrast to their controls. Recently, it was published that LASP-1, on the one hand, is very important for the integrity of the filtration barrier and, on the other

hand, its phosphorylation is regulated by angiotensin II (AngII), leading to relocalization of F-actin fibers and focal adhesions to lamellipodia in cultured podocytes [54]. This underlines the important role of palladin in the localization and function of LASP-1.

We also studied another actin-binding protein, the vasodilator-stimulated phosphoprotein (VASP) for its role on podocyte function. Hohenstein and colleagues have shown that kidney injury is more pronounced in VASP-deficient mice, but surprisingly, long-term disease progression may be protected [55]. Our results revealed a significant downregulation of VASP in PodoPalld129-/- mice of both age groups, suggesting a direct effect of palladin on this protein. This might explain the attenuated phenotype of the PodoPalld129-/- animals. Ezrin, which is specifically expressed in podocytes [56] remained unchanged in PodoPalld129-/- mice at 6 months of age, but a significant downregulation was observed in glomeruli at 12 months of age. Since Wasik et al. has shown that knockdown of ezrin in cultured mouse podocytes leads to reduction of actin stress fibers and cortical actin accumulation at the plasma membrane [57], we hypothesize that downregulation of ezrin in PodoPalld129-/- mice will lead to a weakening of the actin cytoskeleton in podocytes in an age-dependent manner. This is supported by the results of Hugo et al. who observed that after 5/6 nephrectomy, a model for chronic kidney disease, ezrin is downregulated during aging [56].

Another important binding partner of palladin is Pdlim2. Pdlim2 plays a central role as a binding protein for a number of podocyte-essential proteins. As previously shown, Pdlim2 expression was significantly decreased in patients with glomerulopathies [29]. In 6 and 12 months old PodoPalld129-/- mice, we also observed significant downregulation of Pdlim2 protein and mRNA levels. In contrast, Amotl1, a Pdlim2-interacting partner [29], is significantly upregulated in PodoPalld129-/- glomeruli, which might be due to compensation of reduced Pdlim2 expression, as already reported [38]. Pdlim2 seems to be a central protein for podocytes, since a previous study has shown that Pdlim2 expression is closely linked with the expression of the anti-aging protein Klotho [30]. Klotho is significantly reduced in kidneys of patients with chronic renal failure [58]. In line with these findings Klotho is significantly downregulated in 6 and 12 months old PodoPalld129-/- mice. *In vitro* and *in vivo* PAN-induced podocyte injury models showed significant downregulation of Klotho and increased podocyte apoptosis [59]. Neyra and

Hu postulated that Klotho deficiency may be an early biomarker for chronic kidney disease (CKD) and a pathogenic intermediate for CKD development and progression [60].

All together, we show here that palladin, an actin-binding protein, is essential for the intact morphology of the glomerular tuft and podocytes in mice with a 129 genetic background. In addition, palladin regulates the expression of important proteins such as Pdlim2, VASP, Amotl1 and Klotho.

5. Summary

Worldwide, chronic kidney disease is one of the leading public health problems. Podocytes, highly specialized postmitotic cells in the filtration unit of the kidney glomerulus, are essential for the size selectivity of the filtration barrier. Loss of the complex 3D morphology of their interdigitating foot processes, effacement and detachment of the cells from the capillaries lead to proteinuria and often loss of kidney function.

Since the morphology of podocyte foot processes is highly dependent on an intact actin cytoskeleton and actin-binding proteins, we investigated the role of the actin-binding protein palladin in podocytes from mice with a 129 genetic background, that is more susceptible to kidney injury. PodoPalld129-/- mice were examined at 6 and 12 months of age using immunofluorescence staining, electron and 3D super-resolution microscopy as well as qRT-PCR.

Our analysis of PodoPalld129-/- mice at 6 and 12 months of age showed that podocyte-specific knockout of palladin results in dilation of the capillary tuft accompanied by loss of mesangial cells, indicating the influence of palladin on glomerular tuft formation. Besides, we observed morphological abnormalities such as an enlarged sub-podocyte space, cyst formations and an increased number of cell-cell contacts between podocytes and parietal epithelial cells in PodoPalld129-/- mice compared to controls. Moreover, palladin knockout resulted in downregulation of the slit diaphragm protein nephrin as well as an age-dependent significant increase in podocyte foot process effacement. Although there was a significant change in foot process morphology, we did not detect albuminuria in PodoPalld129-/- mice of both age groups. However, we found an increase of trefoil factor 1 (Tff1) in the urine of the mice, indicating an altered, more permeable filtration barrier.

Considering that palladin has several binding sites for important actin-binding and regulatory proteins, we studied the expression of Lasp-1, Pdlim2, VASP and Klotho in dependence on palladin. We found a remarkable reduction in, for example, phosphorylated Lasp-1 as well as Klotho, which could influence the morphology of podocyte foot processes.

Compared with PodoPalldBL/6-/- mice, PodoPalld129-/- mice showed stronger glomerular tuft dilation and developed podocytes with increased morphological abnormalities, underlining the importance of the genetic background.

In conclusion, these results demonstrate the essential role of palladin for podocyte morphology in mice with a 129 genetic background.

6. References

1. Bikbov B, Purcell CA, Levey AS, Smith M, Abdoli A, Abebe M, et al. Global, regional, and national burden of chronic kidney disease, 1990–2017: a systematic analysis for the Global Burden of Disease Study 2017. The Lancet. 2020; 395:709–33. doi: 10.1016/S0140-6736(20)30045-3.

2. Jha V, Garcia-Garcia G, Iseki K, Li Z, Naicker S, Plattner B, et al. Chronic kidney disease: global dimension and perspectives. The Lancet. 2013; 382:260–72. doi: 10.1016/S0140-6736(13)60687-X.

3. Chen TK, Knicely DH, Grams ME. Chronic Kidney Disease Diagnosis and Management: A Review. JAMA. 2019; 322:1294–304. doi: 10.1001/jama.2019.14745 PMID: 31573641.

4. Pavenstädt H, Kriz W, Kretzler M. Cell biology of the glomerular podocyte. Physiol Rev. 2003; 83:253–307. doi: 10.1152/physrev.00020.2002 PMID: 12506131.

5. Ruotsalainen V, Ljungberg P, Wartiovaara J, Lenkkeri U, Kestilä M, Jalanko H, et al. Nephrin is specifically located at the slit diaphragm of glomerular podocytes. Proc Natl Acad Sci U S A. 1999; 96:7962–7. doi: 10.1073/pnas.96.14.7962 PMID: 10393930.

6. Roselli S, Gribouval O, Boute N, Sich M, Benessy F, Attié T, et al. Podocin Localizes in the Kidney to the Slit Diaphragm Area. Am J Pathol. 2002; 160:131–9. doi: 10.1016/S0002-9440(10)64357-X.

7. Daehn IS, Duffield JS. The glomerular filtration barrier: a structural target for novel kidney therapies. Nat Rev Drug Discov. 2021; 20:770–88. Epub 2021/07/14. doi: 10.1038/s41573-021-00242-0 PMID: 34262140.

8. Perico L, Conti S, Benigni A, Remuzzi G. Podocyte-actin dynamics in health and disease. Nat Rev Nephrol. 2016; 12:692–710. Epub 2016/08/30. doi: 10.1038/nrneph.2016.127 PMID: 27573725.

9. Garg P. A Review of Podocyte Biology. Am J Nephrol. 2018; 47 Suppl 1:3–13. Epub 2018/05/31. doi: 10.1159/000481633 PMID: 29852492.

10. Kos CH, Le TC, Sinha S, Henderson JM, Kim SH, Sugimoto H, et al. Mice deficient in α-actinin-4 have severe glomerular disease. J Clin Invest. 2003; 111:1683–90. doi: 10.1172/JCI200317988.

11. Kaplan JM, Kim SH, North KN, Rennke H, Correia LA, Tong HQ, et al. Mutations in ACTN4, encoding alpha-actinin-4, cause familial focal segmental glomerulosclerosis. Nat Genet. 2000; 24:251–6. doi: 10.1038/73456 PMID: 10700177.

12. Michaud J-L. Focal and Segmental Glomerulosclerosis in Mice with Podocyte-Specific Expression of Mutant -Actinin-4. Journal of the American Society of Nephrology. 2003; 14:1200–11. doi: 10.1097/01.ASN.0000059864.88610.5E.

13. Kriz W, Shirato I, Nagata M, LeHir M, Lemley KV. The podocyte's response to stress: the enigma of foot process effacement. Am J Physiol Renal Physiol. 2013; 304:F333-47. doi: 10.1152/ajprenal.00478.2012 PMID: 23235479.

14. Parast MM, Otey CA. Characterization of Palladin, a Novel Protein Localized to Stress Fibers and Cell Adhesions. J Cell Biol. 2000; 150:643–56. doi: 10.1083/jcb.150.3.643.

15. Boukhelifa M. A critical role for palladin in astrocyte morphology and response to injury. Molecular and Cellular Neuroscience. 2003; 23:661–8. doi: 10.1016/S1044-7431(03)00127-1.
16. Rönty M, Taivainen A, Moza M, Otey CA, Carpén O. Molecular analysis of the interaction between palladin and α-actinin. FEBS Letters. 2004; 566:30–4. doi: 10.1016/j.febslet.2004.04.006.
17. Luo H, Liu X, Wang F, Huang Q, Shen S, Wang L, et al. Disruption of palladin results in neural tube closure defects in mice. Molecular and Cellular Neuroscience. 2005; 29:507–15. doi: 10.1016/j.mcn.2004.12.002.
18. Tan J, Chen X-J, Shen C-L, Zhang H-X, Tang L-Y, Lu S-Y, et al. Lacking of palladin leads to multiple cellular events changes which contribute to NTD. Neural Dev. 2017; 12:4. Epub 2017/03/24. doi: 10.1186/s13064-017-0081-6 PMID: 28340616.
19. Rachlin AS, Otey CA. Identification of palladin isoforms and characterization of an isoform-specific interaction between Lasp-1 and palladin. J Cell Sci. 2006; 119:995–1004. doi: 10.1242/jcs.02825 PMID: 16492705.
20. Wang H-V, Moser M. Comparative expression analysis of the murine palladin isoforms. Dev Dyn. 2008; 237:3342–51. doi: 10.1002/dvdy.21755 PMID: 18924229.
21. Dixon RDS, Arneman DK, Rachlin AS, Sundaresan NR, Costello MJ, Campbell SL, et al. Palladin Is an Actin Cross-linking Protein That Uses Immunoglobulin-like Domains to Bind Filamentous Actin. J Biol Chem. 2008; 283:6222–31. doi: 10.1074/jbc.M707694200.
22. Beck MR, Dixon RDS, Goicoechea SM, Murphy GS, Brungardt JG, Beam MT, et al. Structure and function of palladin's actin binding domain. J Mol Biol. 2013; 425:3325–37. doi: 10.1016/j.jmb.2013.06.016 PMID: 23806659.
23. Chew CS, Chen X, Parente JA, Tarrer S, Okamoto C, Qin H-Y. Lasp-1 binds to non-muscle F-actin in vitro and is localized within multiple sites of dynamic actin assembly in vivo. J Cell Sci. 2002; 115:4787–99. doi: 10.1242/jcs.00174 PMID: 12432067.
24. Butt E, Gambaryan S, Göttfert N, Galler A, Marcus K, Meyer HE. Actin binding of human LIM and SH3 protein is regulated by cGMP- and cAMP-dependent protein kinase phosphorylation on serine 146. J Biol Chem. 2003; 278:15601–7. doi: 10.1074/jbc.M209009200 PMID: 12571245.
25. Mykkänen O-M, Grönholm M, Rönty M, Lalowski M, Salmikangas P, Suila H, et al. Characterization of Human Palladin, a Microfilament-associated Protein. MBoC. 2001; 12:3060–73. doi: 10.1091/mbc.12.10.3060.
26. Boukhelifa M, Parast MM, Bear JE, Gertler FB, Otey CA. Palladin is a novel binding partner for Ena/VASP family members. Cell Motil Cytoskeleton. 2004; 58:17–29. doi: 10.1002/cm.10173.
27. Kawaguchi K, Yoshida S, Hatano R, Asano S. Pathophysiological Roles of Ezrin/Radixin/Moesin Proteins. Biol Pharm Bull. 2017; 40:381–90. doi: 10.1248/bpb.b16-01011 PMID: 28381792.
28. Maeda M, Asano E, Ito D, Ito S, Hasegawa Y, Hamaguchi M, et al. Characterization of interaction between CLP36 and palladin. FEBS J. 2009; 276:2775–85. doi: 10.1111/j.1742-4658.2009.07001.x PMID: 19366376.
29. Sistani L, Dunér F, Udumala S, Hultenby K, Uhlen M, Betsholtz C, et al. Pdlim2 is a novel actin-regulating protein of podocyte foot processes. Kidney Int. 2011; 80:1045–54. doi: 10.1038/ki.2011.231 PMID: 21814175.

30. Jin M, Lv P, Chen G, Wang P, Zuo Z, Ren L, et al. Klotho ameliorates cyclosporine A-induced nephropathy via PDLIM2/NF-kB p65 signaling pathway. Biochem Biophys Res Commun. 2017; 486:451–7. doi: 10.1016/j.bbrc.2017.03.061 PMID: 28315683.
31. Endlich N, Schordan E, Cohen CD, Kretzler M, Lewko B, Welsch T, et al. Palladin is a dynamic actin-associated protein in podocytes. Kidney Int. 2009; 75:214–26. doi: 10.1038/ki.2008.486 PMID: 19116644.
32. Artelt N, Ludwig TA, Rogge H, Kavvadas P, Siegerist F, Blumenthal A, et al. The Role of Palladin in Podocytes. J Am Soc Nephrol. 2018; 29:1662–78. doi: 10.1681/ASN.2017091039 PMID: 29720549.
33. Ma L-J, Fogo AB. Model of robust induction of glomerulosclerosis in mice: importance of genetic background. Kidney Int. 2003; 64:350–5. doi: 10.1046/j.1523-1755.2003.00058.x PMID: 12787428.
34. Hartner A, Cordasic N, Klanke B, Veelken R, Hilgers KF. Strain differences in the development of hypertension and glomerular lesions induced by deoxycorticosterone acetate salt in mice. Nephrol Dial Transplant. 2003; 18:1999–2004. doi: 10.1093/ndt/gfg299 PMID: 13679473.
35. Ishola DA, van der Giezen DM, Hahnel B, Goldschmeding R, Kriz W, Koomans HA, et al. In mice, proteinuria and renal inflammatory responses to albumin overload are strain-dependent. Nephrol Dial Transplant. 2006; 21:591–7. doi: 10.1093/ndt/gfi303 PMID: 16326737.
36. Qi Z, Fujita H, Jin J, Davis LS, Wang Y, Fogo AB, et al. Characterization of Susceptibility of Inbred Mouse Strains to Diabetic Nephropathy. Diabetes. 2005; 54:2628–37. doi: 10.2337/diabetes.54.9.2628.
37. Wong GT. Speed congenics: applications for transgenic and knock-out mouse strains. Neuropeptides. 2002; 36:230–6. doi: 10.1054/npep.2002.0905 PMID: 12359513.
38. Artelt N, Ritter AM, Leitermann L, Kliewe F, Schlüter R, Simm S, et al. The podocyte-specific knockout of palladin in mice with a 129 genetic background affects podocyte morphology and the expression of palladin interacting proteins. PLoS ONE. 2021; 16:e0260878. Epub 2021/12/08. doi: 10.1371/journal.pone.0260878 PMID: 34879092.
39. Artelt N, Siegerist F, Ritter AM, Grisk O, Schlüter R, Endlich K, et al. Comparative Analysis of Podocyte Foot Process Morphology in Three Species by 3D Super-Resolution Microscopy. Front Med (Lausanne). 2018; 5:292. doi: 10.3389/fmed.2018.00292 PMID: 30425988.
40. Schindelin J, Arganda-Carreras I, Frise E, Kaynig V, Longair M, Pietzsch T, et al. Fiji: an open-source platform for biological-image analysis. Nat Methods. 2012; 9:676–82. Epub 2012/06/28. doi: 10.1038/nmeth.2019 PMID: 22743772.
41. Steppan J, Jandu S, Wang H, Kang S, Savage W, Narayanan R, et al. Commonly used mouse strains have distinct vascular properties. Hypertens Res. 2020; 43:1175–81. Epub 2020/05/14. doi: 10.1038/s41440-020-0467-4 PMID: 32409775.
42. Wiggins JE. Aging in the glomerulus. J Gerontol A Biol Sci Med Sci. 2012; 67:1358–64. Epub 2012/07/25. doi: 10.1093/gerona/gls157 PMID: 22843670.
43. Fang Y, Gong AY, Haller ST, Dworkin LD, Liu Z, Gong R. The ageing kidney: Molecular mechanisms and clinical implications. Ageing Res Rev. 2020; 63:101151. Epub 2020/08/22. doi: 10.1016/j.arr.2020.101151 PMID: 32835891.

44. Weinstein JR, Anderson S. The aging kidney: physiological changes. Adv Chronic Kidney Dis. 2010; 17:302–7. doi: 10.1053/j.ackd.2010.05.002 PMID: 20610357.
45. Schlöndorff D, Banas B. The mesangial cell revisited: no cell is an island. J Am Soc Nephrol. 2009; 20:1179–87. doi: 10.1681/ASN.2008050549 PMID: 19470685.
46. Hartner A, Schöcklmann H, Pröls F, Müller U, Sterzel RB. Alpha8 integrin in glomerular mesangial cells and in experimental glomerulonephritis. Kidney Int. 1999; 56:1468–80. doi: 10.1046/j.1523-1755.1999.00662.x PMID: 10504498.
47. Eremina V, Cui S, Gerber H, Ferrara N, Haigh J, Nagy A, et al. Vascular endothelial growth factor a signaling in the podocyte-endothelial compartment is required for mesangial cell migration and survival. J Am Soc Nephrol. 2006; 17:724–35. Epub 2006/01/25. doi: 10.1681/ASN.2005080810 PMID: 16436493.
48. Kriz W. Maintenance and Breakdown of Glomerular Tuft Architecture. J Am Soc Nephrol. 2018; 29:1075–7. doi: 10.1681/ASN.2018020200 PMID: 29535166.
49. Smeets B, Moeller MJ. Parietal epithelial cells and podocytes in glomerular diseases. Semin Nephrol. 2012; 32:357–67. doi: 10.1016/j.semnephrol.2012.06.007 PMID: 22958490.
50. Gurung R, Yadav R, Brungardt JG, Orlova A, Egelman EH, Beck MR. Actin polymerization is stimulated by actin cross-linking protein palladin. Biochem J. 2016; 473:383–96. Epub 2015/11/25. doi: 10.1042/BJ20151050 PMID: 26607837.
51. Kliewe F, Kaling S, Lötzsch H, Artelt N, Schindler M, Rogge H, et al. Fibronectin is up-regulated in podocytes by mechanical stress. FASEB J. 2019; 33:14450–60. Epub 2019/11/01. doi: 10.1096/fj.201900978RR PMID: 31675484.
52. Dickson LE, Wagner MC, Sandoval RM, Molitoris BA. The proximal tubule and albuminuria: really! J Am Soc Nephrol. 2014; 25:443–53. doi: 10.1681/ASN.2013090950 PMID: 24408874.
53. Lebherz-Eichinger D, Tudor B, Ankersmit HJ, Reiter T, Haas M, Roth-Walter F, et al. Trefoil Factor 1 Excretion Is Increased in Early Stages of Chronic Kidney Disease. PLoS ONE. 2015; 10:e0138312. doi: 10.1371/journal.pone.0138312 PMID: 26390128.
54. Lepa C, Möller-Kerutt A, Stölting M, Picciotto C, Eddy M-L, Butt E, et al. LIM and SH3 protein 1 (LASP-1): A novel link between the slit membrane and actin cytoskeleton dynamics in podocytes. FASEB J. 2020; 34:5453–64. Epub 2020/02/21. doi: 10.1096/fj.201901443R PMID: 32086849.
55. Hohenstein B, Kasperek L, Kobelt D-J, Daniel C, Gambaryan S, Renné T, et al. Vasodilator-stimulated phosphoprotein-deficient mice demonstrate increased platelet activation but improved renal endothelial preservation and regeneration in passive nephrotoxic nephritis. J Am Soc Nephrol. 2005; 16:986–96. doi: 10.1681/ASN.2004070591 PMID: 15743999.
56. Hugo C, Nangaku M, Shankland SJ, Pichler R, Gordon K, Amieva MR, et al. The plasma membrane-actin linking protein, ezrin, is a glomerular epithelial cell marker in glomerulogenesis, in the adult kidney and in glomerular injury. Kidney Int. 1998; 54:1934–44. doi: 10.1046/j.1523-1755.1998.00195.x PMID: 9853258.
57. Wasik AA, Koskelainen S, Hyvönen ME, Musante L, Lehtonen E, Koskenniemi K, et al. Ezrin is down-regulated in diabetic kidney glomeruli and regulates actin reorganization and glucose uptake via GLUT1 in cultured podocytes. Am J Pathol. 2014; 184:1727–39. doi: 10.1016/j.ajpath.2014.03.002 PMID: 24726496.
58. Koh N, Fujimori T, Nishiguchi S, Tamori A, Shiomi S, Nakatani T, et al. Severely reduced production of klotho in human chronic renal failure kidney. Biochem

Biophys Res Commun. 2001; 280:1015–20. doi: 10.1006/bbrc.2000.4226 PMID: 11162628.

59. Qiu X, Huo J, Xia S, Zhao W, Luo Y, Xia Y. Dysfunction of the Klotho-miR-30s/TRPC6 axis confers podocyte injury. Biochem Biophys Res Commun. 2021; 557:90–6. Epub 2021/04/13. doi: 10.1016/j.bbrc.2021.04.003 PMID: 33862465.

60. Neyra JA, Hu MC. Potential application of klotho in human chronic kidney disease. Bone. 2017; 100:41–9. doi: 10.1016/j.bone.2017.01.017 PMID: 28115282.

7. Appendix

7.1 Artelt et al., *Frontiers in Medicine*. 2018

frontiers in Medicine

BRIEF RESEARCH REPORT
published: 30 October 2018
doi: 10.3389/fmed.2018.00292

Comparative Analysis of Podocyte Foot Process Morphology in Three Species by 3D Super-Resolution Microscopy

Nadine Artelt[1], Florian Siegerist[1†], Alina M. Ritter[1], Olaf Grisk[2], Rabea Schlüter[3], Karlhans Endlich[1†] and Nicole Endlich[1]*

[1] Institute for Anatomy and Cell Biology, University Medicine Greifswald, Greifswald, Germany, [2] Institute for Physiology, University Medicine Greifswald, Karlsburg, Germany, [3] Imaging Center of the Department of Biology, University of Greifswald, Greifswald, Germany

OPEN ACCESS

Edited by:
Astrid Weins,
Harvard Medical School,
United States

Reviewed by:
Kirk Campbell,
Icahn School of Medicine at Mount Sinai, United States
Deepak Nihalani,
Medical University of South Carolina, United States

****Correspondence:***
Nicole Endlich
nicole.endlich@uni-greifswald.de

[†]Florian Siegerist
orcid.org/0000-0003-1629-4982
Karlhans Endlich
orcid.org/0000-0001-6052-6061

Specialty section:
This article was submitted to Nephrology, a section of the journal Frontiers in Medicine

Received: *29 June 2018*
Accepted: *25 September 2018*
Published: *30 October 2018*

Citation:
Artelt N, Siegerist F, Ritter AM, Grisk O, Schlüter R, Endlich K and Endlich N (2018) Comparative Analysis of Podocyte Foot Process Morphology in Three Species by 3D Super-Resolution Microscopy. Front. Med. 5:292. doi: 10.3389/fmed.2018.00292

Since the size selectivity of the filtration barrier and kidney function are highly dependent on podocyte foot process morphology, visualization of foot processes is important. However, the size of foot processes is below the optical resolution of light microscopy. Therefore, electron microcopy has been indispensable to detect changes in foot process morphology so far, but it is a sophisticated and time-consuming technique. Recently, our group has shown that 3D structured illumination microscopy (3D-SIM), a super-resolution microscopy (SRM) technique, can visualize individual foot processes in human biopsies. Moreover, we have developed a software-based approach to directly quantify the structure of podocyte foot processes named *Podocyte Exact Morphology Measurement Procedure (PEMP)*. As shown in patients suffering from minimal change disease (MCD), PEMP allows the quantification of changes of the foot process morphology by measuring the filtration slit density (FSD). Since rodents are frequently used in basic research, we have applied PEMP to quantify foot processes of mice and rats. Comparative analysis of nephrin-stained kidneys from humans, rats, and mice showed significant differences of the FSD. The highest FSD was measured in mice ($3.83 \pm 0.37\ \mu m^{-1}$; mean ± SD) followed by rats ($3.36 \pm 0.42\ \mu m^{-1}$) and humans ($3.11 \pm 0.26\ \mu m^{-1}$). To demonstrate that PEMP can be used to determine foot process morphology also in affected animals, we measured the FSD in palladin-knockout mice on a 129S1 genetic background compared to wild-type littermates. Taken together, we established a method for the quick and exact quantification of podocyte foot process morphology which can be applied to diagnosis and basic research.

Keywords: super-resolution microscopy, nephrin, slit diaphragm, podocyte foot process morphology, effacement

INTRODUCTION

Since the function of the filtration barrier is dependent on podocyte foot process morphology, ultrastructural analyses of kidney biopsies as well as of kidney sections of animal models are important. However, the size of podocyte foot processes and the slit diaphragm in between is below the optical resolution limit of light microscopy and therefore electron microscopy (EM) had to be

used for analysis in the past. However, ultrastructural evaluation of the podocyte morphology by EM has some disadvantages: On one hand, the preparation procedure is very sophisticated as well as time consuming and generates a bias due to a dependence on the sectioning angle of the probe (1). On the other hand, the analysis is only subjective and qualitative and represents only a small area of the total kidney section.

Recently, it has been demonstrated that super-resolution microscopy (SRM) overcomes the optical resolution limit of 200 nm formulated by Ernst Abbe. Therefore, different research groups have focused their attention on the visualization of podocyte foot processes by SRM (2, 3). The term SRM summarizes a variety of different techniques like photo-activated localization microscopy (PALM), (direct) stochastic optical reconstruction microscopy [(d)STORM], stimulated emission depletion (STED) and structured illumination microscopy (SIM). SIM is the technique with the lowest optical resolution (85–100 nm in x,y-plane) of all SRM techniques. It allows using standard preparation procedures, normal dyes and mounting media. Furthermore, 3-dimensional structured illumination microscopy (3D-SIM) can be performed with a resolution in the z-plane of 300 nm.

The technique of SIM is based on the generation of Moiré patterns by illuminating the sample through a grid, which is shifted and rotated. Moiré patterns change the spatial frequencies in such a way that the optical resolution is doubled. To generate a SIM picture, three to five different angles and five phase shifts of the grid are necessary resulting in 15–25 widefield (WF) pictures that can be reconstructed by a specific algorithm to extract the high-frequency information into a high-resolution picture (4, 5). We have already visualized and measured individual podocyte foot processes in formalin-fixed and paraffin-embedded (FFPE) human tissue originating from healthy subjects and patients diagnosed for minimal change disease (MCD) by SIM (6). Further, we have established an automatic evaluation of the filtration slit density (FSD), meaning the total length of the slit diaphragm per glomerular capillary area, as a direct parameter to quantify podocyte morphology (6). In combination with classic histology of FFPE sections, the approach named *Podocyte Exact Morphology Measurement Procedure (PEMP)* is able to diagnose MCD along with the quantification of the severity of podocyte injury.

It is well known that foot process morphology is highly dependent on an intact actin cytoskeleton. In this context, mutations in actin-binding proteins that are specifically expressed in podocytes, like α-actinin-4 (7) or anillin (8), induce focal segmental glomerulosclerosis (FSGS). Since the actin-associated protein palladin is highly expressed in podocytes (9), a podocyte-specific knockout mouse was generated (10). In these mice, we found alterations in podocyte morphology as well as an increased susceptibility to develop glomerulopathies compared with wild type mice in response to the injection of nephrotoxic serum (10).

The following study determined the FSD of human, rat and mouse podocytes that were stained for nephrin and the actin-binding protein synaptopodin by 3D-SIM. Furthermore, we quantified the broadening of the podocyte foot processes of palladin-knockout mice (6- and 12-month) backcrossed to a 129S1 background (PodoPalld129$^{-/-}$) compared to control mice by PEMP.

MATERIALS AND METHODS

Animal Experiments

All studies involving experimental animals were performed in accordance with the German animal protection act and overseen by local authorities of the federal state Mecklenburg-Western Pomerania. Rat kidney tissue from 4-month-old male Wistar rats (Charles River, Sulzfeld, Germany) was used. The animals were kept with humidity (60%) and temperature (22°C) controlled and 12 h day/night cycle. Food and fresh tap water were available *ad libitum*. Rat kidneys were fixed in 4% paraformaldehyde and after dehydration in a graded series in ethanol and clearing in xylene embedded in paraffin. Mice were housed as described previously (11). Podocyte-specific palladin-knockout (PodoPalldBL6$^{-/-}$) mice and controls (PodoPalldBL6$^{+/+}$) with C57BL/6 genetic background were generated as described previously (10) and isolation of glomeruli of 6 month old male mice with magnetic Dynabeads was performed as described before (12). Mice were backcrossed to the 129S1 genetic background and male podocyte-specific palladin-knockout (PodoPalld129$^{-/-}$) and control (PodoPalld129$^{+/+}$) mice were used for 3D-SIM at 6 months and 1 year of age. Genotyping of mice was performed with Phire® Animal Tissue Direct PCR Kit (Finnzymes/Thermo Fisher Scientific, Waltham; MA, USA) in accordance to the manufacturer's instructions using specific primers (10).

Human Biopsies

As healthy controls, anonymized formalin-fixed and paraffin-embedded excess kidney tissue of partial nephrectomies of the Department of Urology of the University Medicine Greifswald was used. The local ethics committee of the University Medicine Greifswald approved the use of the biopsies from Greifswald. All experiments were performed in accordance with local guidelines overseen by the University Medicine Greifswald, Greifswald, Mecklenburg-Western Pomerania.

3D-SIM

Sample preparation and imaging was performed as described before (6) with following minor adjustments: 4 µm paraffin sections were directly mounted on #1.5 high precision coverslips (VWR, Radnor, PA, USA) and paraformaldehyde-induced autofluorescence was quenched by incubation for 10 min in 100 mM glycine dissolved in 1x PBS, pH 7.4. Sections were blocked in 1% fetal bovine serum, 1% normal goat serum, 1% bovine serum albumin, and 0.1% cold fish gelatin in PBS for 1 h at room temperature. Primary antibodies diluted in blocking solution were: 1:300 polyclonal guinea pig anti nephrin antiserum (GP-N2), 1:50 monoclonal mouse anti synaptopodin IgG1 antibody (G1D4) (both Progen, Heidelberg, Germany), 1:150 polyclonal rabbit anti synaptopodin IgG (SE-19), 1:150 monoclonal mouse anti α-tubulin IgG1 antibody (T9026) (both Sigma-Aldrich, St. Louis, MO, USA) detected by Cy3-labeled polyclonal donkey anti guinea pig IgG, Alexa

488-labeled goat anti mouse IgG F(ab)$_2$ fragment and Cy3-labeled polyclonal goat anti rabbit IgG (H+L) (all from Jackson Immuno Research, Hamburg, Germany) diluted 1:600 in blocking solution. Nuclei were stained for 5 min with DAPI (1:100, Sigma-Aldrich) diluted in PBS. Samples were mounted in Mowiol for microscopy (Carl Roth, Karlsruhe, Germany). WF and 3D-SIM images were acquired on a Zeiss Elyra PS.1 system with five horizontal shifts and five rotations of the illumination pattern with a slice-to-slice distance of 110 nm. 3D-SIM images were reconstructed using Zeiss ZEN black software. To account for chromatic aberration of the optical system, channels were three-dimensionally aligned using values determined by imaging of sub-diffraction fluorescent beads (Tetraspek beads, Molecular Probes, Invitrogen) mounted in the same medium as the biological samples. CLSM micrographs were obtained on a Leica TCS SP5 laser scanning system using a 63x, 1.4 NA oil immersion objective. Digital post-processing, profile plotting and *PEMP* was performed using FIJI (13) combined with the custom-built macro described before (6). Briefly, PEMP was performed on 3D-SIM images of nephrin-stained kidney sections. Areas of the capillary were selected and encircled. The software program determined the total slit diaphragm length (lSD) and the capillary area (A) of the selected region. FSD values were calculated from the ratio of the lSD and A. The following image stacks were analyzed by PEMP: 21–30 glomeruli in three individual rats, 30 glomeruli in four individual humans and 20 glomeruli in three to four individual PodoPalld129$^{+/+}$ and PodoPalld129$^{-/-}$ mice. Student's *t*-test with Bonferroni correction for multiple testing and two-way analysis of variance were used for statistical analysis. Differences were regarded as significant at a $p < 0.05$

Scanning Electron Microscopy (SEM)

Glomeruli of 6 month old male PodoPalld$^{+/+}$ and PodoPalld$^{-/-}$ mice were isolated with magnetic Dynabeads as described previously (12). Samples were fixed with 2.5% glutaraldehyde in PBS (pH 7.5) for 1 h at room temperature and then stored at 4°C overnight. After washing with 1x PBS, samples were treated with 1% osmium tetroxide in PBS for 1 h, 1% thiocarbohydrazide for 30 min, and 1% osmium tetroxide in PBS for 1 h at room temperature with washing steps in between. Subsequently, samples were dehydrated in a graded series of aqueous ethanol solutions (10–100%) and then critical point-dried. Finally, samples were mounted on aluminum stubs, sputtered with gold/palladium and examined with a scanning electron microscope EVO LS10 (Carl Zeiss Microscopy GmbH, Oberkochen, Germany). Afterwards, micrographs were edited using Adobe Photoshop CS6.

RESULTS

Visualization of Podocyte Foot Processes by Widefield Microscopy, Confocal Laser Scanning Microscopy, and 3D-SIM

To demonstrate the increase of the optical resolution by SIM, we imaged immobilized sub-diffraction fluorescent beads by WF and 3D-SIM and measured the full width at the half maximum of the fluorescence intensity (FWHM). As shown in the graph in **Figure 1A**, our optic setup was able to reach a lateral resolution of ∼105 nm.

Four micrometers of FFPE sections of rat kidneys were incubated with antibodies against the slit diaphragm protein nephrin as well as the actin-associated, foot process-specific protein synaptopodin. After staining with the secondary antibodies labeled with Cy3- and Alexa 488, respectively, the kidney sections were visualized by confocal laser scanning microscopy (CLSM), WF microscopy and finally by 3D-SIM. **Figure 1B** demonstrates that the 3D-SIM images of healthy rat glomeruli show the slit diaphragm (purple) in high resolution as well as the interdigitating foot processes (green) in contrast to images taken by CLSM and WF with a much lower resolution.

Additionally, rat kidney sections were co-stained with an antibody against synaptopodin and the microtubule protein α-tubulin (**Supplementary Figure 1**, **Supplementary Movie 1**). 3D-SIM images display the highest resolution of glomerular capillaries surrounded by α-tubulin-positive major processes next to podocyte foot processes stained with synaptopodin.

Comparative Analysis of Foot Process Morphology in Humans, Rats and Mice

In **Figure 1C**, the corresponding 3D-SIM images of all three healthy species are shown. In humans as well as in rats and mice, the interdigitating synaptopodin-labeled foot processes and the nephrin-positive slit diaphragm can be clearly distinguished. 3D-SIM is therefore able to at least double the optical resolution allowing the study of foot processes and the slit diaphragm in detail.

To compare podocyte foot process morphology of humans, rats and mice, 3D-SIM of stained tissue (nephrin and synaptopodin) was performed. As shown in **Figure 1C**, human, rat and mouse kidney sections show interdigitating foot processes stained for synaptopodin (green) which are bridged by the slit diaphragm protein nephrin (purple). The individual foot processes of all species were clearly distinguishable from the slit diaphragm. The interdigitating nature of foot processes is also demonstrated by rectangular profile plots over several foot processes demonstrating synaptopodin-fluorescence peak values in areas where no signal for nephrin is detected and vice versa.

Furthermore, we applied our recently developed image processing procedure named PEMP to automatically quantify the changes of the podocyte morphology under different conditions. Using PEMP, the slit diaphragm is automatically segmented (red lines in **Figure 2B**) in the region of interest (marked by yellow border) and the length of the filtration slit per glomerular capillary area is determined (**Figures 2A,B**). The ratio of both values is described as the FSD which inversely correlates with the width of podocytes foot processes (d_{FP}) (6). The graph in **Figure 2C** shows the corresponding mean FSD values of the three different species investigated in this study. In human biopsies, we measured a mean FSD of $3.11 \pm 0.26\ \mu m^{-1}$ (mean ± SD, $n = 121$ glomeruli of four humans), whereas rats and mice showed a statistically significant higher FSD of $3.36 \pm 0.42\ \mu m^{-1}$ ($n = 75$

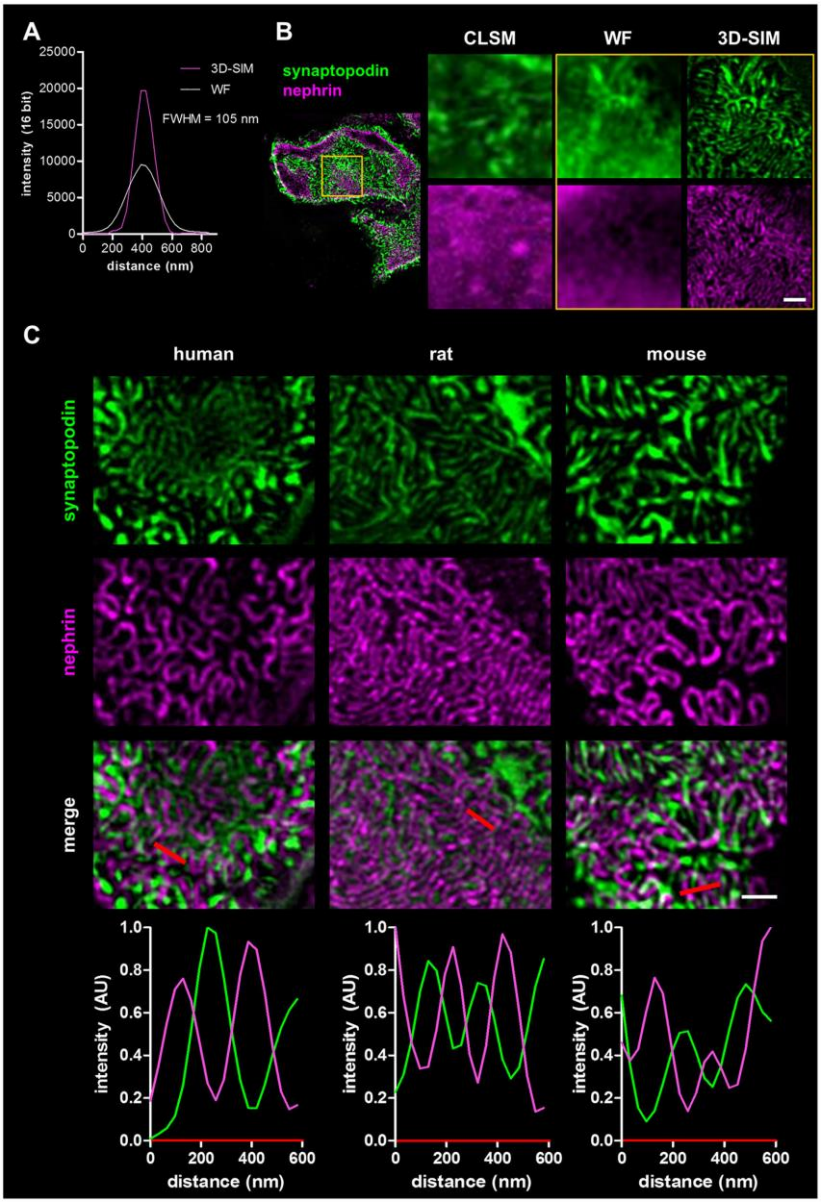

FIGURE 1 | Panel **(A)** shows the resolution of fluorescent beads imaged by wide field (WF) and 3-D structured illumination microscopy (3D-SIM). Panel **(B)** compares the resolution of a healthy rat capillary loop in the glomerulus stained for synaptopodin and nephrin imaged by confocal laser scanning microscopy (CLSM), WF, and 3D-SIM (yellow box). Scale bar represents 1 μm. Panel **(C)** shows synaptopodin and nephrin stained kidney sections of healthy human, rat and mouse. Corresponding intensity profile plots over several foot processes (red lines) are shown at the bottom. Scale bar represents 1 μm.

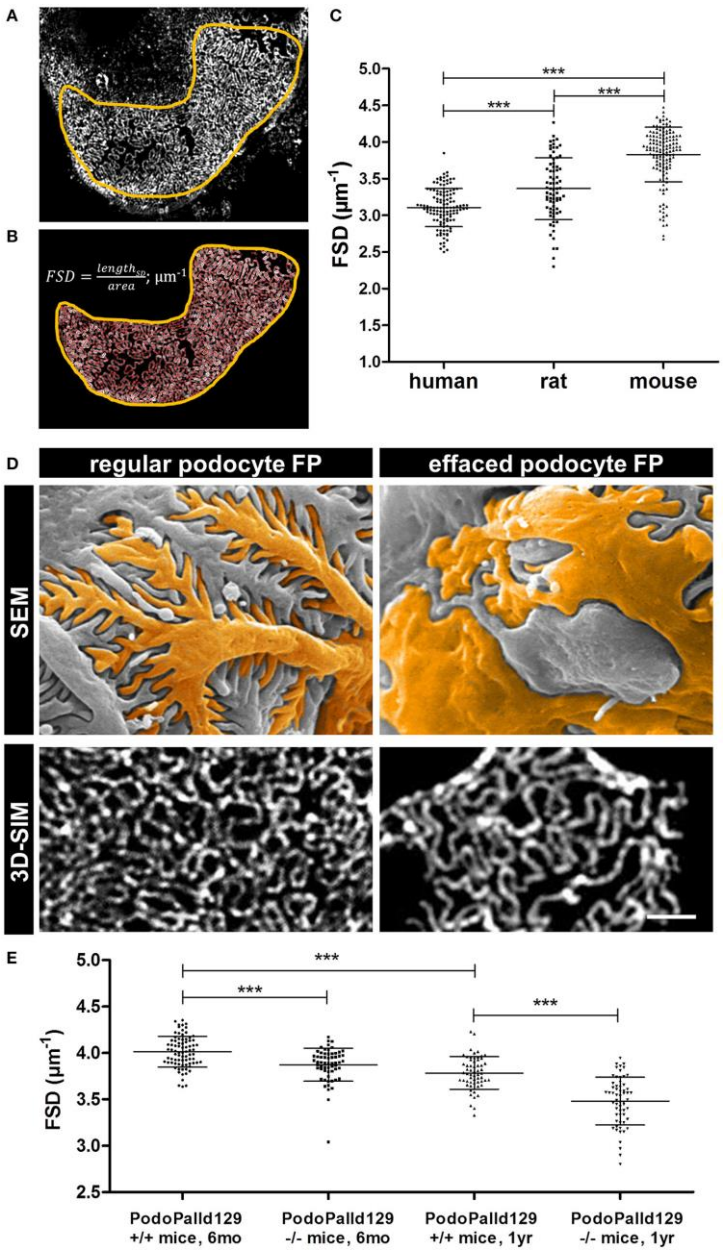

FIGURE 2 | Panel **(A)** shows a murine glomerular capillary area with clearly distinguishable foot processes. Panel **(B)** shows the PEMP principle of automatic segmentation (red) of the slit diaphragm length and quantification of the glomerular capillary area (yellow). The graph in **(C)** shows FSD values of healthy human, rat,

(Continued)

FIGURE 2 | and mouse tissue. Horizontal bars indicate mean values; whiskers show the corresponding standard deviations. ***$p < 0.0005$. Panel **(D)** demonstrates regular and effaced podocyte foot processes (FP) of 6 month old control (PodoPalld$^{+/+}$) and podocyte-specific palladin-knockout mice (PodoPalld$^{-/-}$). Upper panels display images taken by scanning electron microscopy (SEM) and were false colored for better visualization. Images below display kidney sections stained for the slit diaphragm protein nephrin imaged by 3D-SIM. Scale bar represents 1 μm. FSD values of 6 month and 1 year old 129S1 control mice (PodoPalld129$^{+/+}$) and 129S1 podocyte-specific palladin-knockout (PodoPalld129$^{-/-}$) mice are shown in **(E)**. Horizontal bars indicate mean values, whiskers show the corresponding standard deviations. ***$p < 0.001$.

glomeruli of three rats) and $3.83 \pm 0.37\ \mu m^{-1}$ ($n = 138$ glomeruli of six mice), respectively.

Quantification of Podocyte Effacement in Podocyte-Specific Palladin-Knockout Mice on the 129S1 Background

Figure 2D shows regular podocytes with well-organized and interdigitating foot processes in scanning electron microscopy (SEM) and a nicely formed slit diaphragm, stained for nephrin, in 3D-SIM. In comparison, injured podocytes with effaced foot processes have broadened podocyte foot processes as shown by SEM and 3D-SIM which visualizes a disorganized pattern of the slit diaphragm.

To check whether PEMP is a method to quantify podocyte injury in animal models, we analyzed 3D-SIM images of podocyte-specific palladin knockout mice on a 129S1 background (PodoPalld129$^{-/-}$ mice). **Figure 2E** shows the comparison of the mean FSD of PodoPalld129$^{-/-}$ mice at different ages to the corresponding controls (PodoPalld129$^{+/+}$). Genotype and age both significantly affected FSD. We observed that PodoPalld129$^{-/-}$ mice possess a significantly lower FSD ($3.87 \pm 0.02\ \mu m^{-1}$; mean ± SEM, $n = 60$ glomeruli of three animals $p < 0.001$) compared to PodoPalld129$^{+/+}$ mice ($4.01 \pm 0.02\ \mu m^{-1}$; $n = 80$ glomeruli of four animals) at the age of 6 months. At the age of 12 months, this difference further increased and the FSD for PodoPalld129$^{-/-}$ mice was $3.48 \pm 0.03\ \mu m^{-1}$ ($n = 60$ glomeruli of three animals) in contrast to $3.78 \pm 0.02\ \mu m^{-1}$ ($n = 60$ glomeruli of three animals, $p < 0.001$) in PodoPalld129$^{+/+}$ mice. Interestingly, we also observed a significant difference ($p < 0.001$) between the FSD values in PodoPalld129$^{+/+}$ at the age of 6 vs. 12 month indicating that PEMP can quantify also slight differences of podocyte foot process morphology.

DISCUSSION

In the past, high resolution visualization of podocyte foot processes as well as of the slit diaphragm spanned between the interdigitating foot processes was only possible by electron microscopy (EM), a very sophisticated and time-consuming technique. Quantification of the foot processes by EM is challenging because this technique allows only the preparation of very thin and small kidney sections. On the other hand, the values obtained by EM highly depend on the sectioning angle of the glomerular capillary. Areas with broadened foot processes, due to sectioning of foot processes along their longitudinal axis, cannot be distinguished from truly effaced areas and lead to false values of foot process morphology as already shown by our group (6). Therefore, the EM results do not correctly represent the real podocyte morphology of biopsies and kidneys taken from patients or animal models, respectively. However, EM analysis remains still valuable for assessing ultrastructural details of podocytes, e.g., the subpodocyte space.

With the development of a new light microscopy technique, the SRM, a new era also for podocyte foot process morphology analysis has started. In contrast to other light microscopy techniques, like CLSM and WF, which allow only a blurred view on foot process morphology and do not reveal any details about the slit diaphragm due to the optical limitation described by Ernst Abbe, a specific type of SRM namely 3D-SIM enabled us to study the course of the slit diaphragm in greater detail. In contrast to STED, another SRM technique allowing an optical resolution down to even 35 nm, 3D-SIM can be directly applied on standard biopsy sections used in pathology routine without any time-consuming optical clearing. Recently, Suleiman and colleagues used Airyscan microscopy to image podocytes of whole murine isolated glomeruli *in situ* stained for synaptopodin (2). As an alternative to SIM, Airyscan has a resolution of 120 nm in the xy-plane and 350 nm in the z-direction, a resolution between that of CLSM and 3D-SIM (14).

Another method to overcome the optical resolution limit was conceived by Grgic and colleagues who imaged individual foot processes in mice carrying an inducible reporter transgene allowing for tamoxifen dose-dependent tomato-expression in podocytes (15). The resolution of CLSM was sufficient to visualize major processes and foot processes, if a labeled podocyte contacted a non-labeled podocyte (15). In that case, the space between single tomato-labeled and non-fluorescent foot processes can be visualized. However, if labeling is to dense, imaging will not work, as only the sub-diffraction and non-fluorescent slit diaphragm (∼30 nm) surrounds foot processes. In 2013, Höhne and colleagues overcame this limitation using a similar approach. They modified the mouse model as they used a confetti reporter approach to label neighboring podocytes in different colors (16). In doing so, the researchers showed regularly interdigitating foot processes of adjacent podocytes in isolated murine glomeruli by CLSM. However, this method works only with transgenic animals and cannot be translated to normal mouse, rat, und human kidney tissue.

In the past another SRM technique, (d)STORM, was used to study details of podocyte foot process morphology and podocyte-associated proteins (2). However, only cryosections and specific dyes that can be transferred in a so-called dark state can be used. Further, the quality of the results is highly dependent on the redox buffer system which has to be optimized for each fluorescent dye. Moreover, this technique cannot be used to quantify or to compare morphological changes of foot processes

and the slit diaphragm, respectively, in a larger number of animals and biopsies. However, this would be the prerequisite for the pathological routine.

Since some kidney diseases like congenital FSGS are associated with a down regulation of the slit diaphragm protein nephrin (17, 18), alternative slit diaphragm markers like podocin can be used as it was nicely demonstrated by Unnersjö-Jess et al. (3) in a STED-based work on optical cleared kidneys.

The complex podocyte morphology is highly dependent on the actin cytoskeleton and the organization by actin-associated proteins. We have recently shown that palladin, an actin-binding protein (9), plays a pivotal role for the dynamics of the actin cytoskeleton as well as for the stabilization of actin filaments. PEMP analysis of podocyte-specific palladin knockout mice on a specific genetic background (129S1) showed at 6 months as well as at 1 year of age a significant reduction of the FSD compared to the littermates. Moreover, 12-month-old control mice showed significantly more effaced podocyte foot processes compared to mice at 6 months of age, meaning that aging alters podocyte foot process morphology in mice. This is in agreement with the observation of Hassan and colleagues who have already described an age-dependent increase of foot process effacement in podocyte-specific *Sec63/Xbp1* knockout mice in a non-quantitative fashion (19).

Taken together, PEMP is an excellent tool to easily measure podocyte foot process morphology of various species in an exact and quantitative way.

ETHICS STATEMENT

This study was carried out in accordance with the recommendations of local guidelines, local ethics committee of the University Medicine Greifswald with written informed consent from all subjects. All subjects gave written informed consent in accordance with the Declaration of Helsinki. The protocol was approved by the University Medicine Greifswald. This study was carried out in accordance with the recommendations of national animal protection guidelines, National Institutes of Health Guide for the Care and Use of Laboratory Animals. The protocol was approved by the local governmental authorities.

AUTHOR CONTRIBUTIONS

The study was designed by NA, FS, KE, and NE. NA and FS compared the resolution of confocal laser scanning microscopy, wide field, and 3D-SIM. FS conducted comparative analysis of podocyte foot process morphology in humans, rats and mice. NA and AR performed PEMP in PodoPalld129 mice. Scanning electron microscopy was performed by NA and RS. OG provided rat kidney samples. NA, FS, NE, and KE wrote the manuscript. All authors reviewed the manuscript.

FUNDING

This study was supported by a grant of the German Research Foundation (DFG, grant INST 2026/13-1, FUGG) to KE and NE and by a grant of the Federal Ministry of Education and Research (BMBF, grant 01GM1518B, STOP-FSGS) to NE.

SUPPLEMENTARY MATERIAL

The Supplementary Material for this article can be found online at: https://www.frontiersin.org/articles/10.3389/fmed.2018.00292/full#supplementary-material

REFERENCES

1. Gundersen HJ, Seefeldt T, Osterby R. Glomerular epithelial foot processes in normal man and rats. Distribution of true width and its intra- and inter-individual variation. *Cell Tissue Res.* (1980) 205:147–55. doi: 10.1007/BF00234450
2. Suleiman HY, Roth R, Jain S, Heuser JE, Shaw AS, Miner JH. Injury-induced actin cytoskeleton reorganization in podocytes revealed by super-resolution microscopy. *JCI Insight* (2017) 2:94137. doi: 10.1172/jci.insight.94137
3. Unnersjö-Jess D, Scott L, Blom H, Brismar H. Super-resolution stimulated emission depletion imaging of slit diaphragm proteins in optically cleared kidney tissue. *Kidney Int.* (2016) 89:243–7. doi: 10.1038/ki.2015.308
4. Gustafsson MG, Shao L, Carlton PM, Wang CJ, Golubovskaya IN, Cande WZ, et al. Three-dimensional resolution doubling in wide-field fluorescence microscopy by structured illumination. *Biophys J.* (2008) 94:4957–70. doi: 10.1529/biophysj.107.120345
5. Gustafsson MG. Surpassing the lateral resolution limit by a factor of two using structured illumination microscopy. *J Microsc.* (2000) 198:82–7. doi: 10.1046/j.1365-2818.2000.00710.x
6. Siegerist F, Ribback S, Dombrowski F, Amann K, Zimmermann U, Endlich K, et al. Structured illumination microscopy and automatized image processing as a rapid diagnostic tool for podocyte effacement. *Sci Rep.* (2017) 7:11473. doi: 10.1038/s41598-017-11553-x
7. Kaplan JM, Kim SH, North KN, Rennke H, Correia LA, Tong HQ, et al. Mutations in ACTN4, encoding alpha-actinin-4, cause familial focal segmental glomerulosclerosis. *Nat Genet.* (2000) 24:251–6. doi: 10.1038/73456
8. Gbadegesin RA, Hall G, Adeyemo A, Hanke N, Tossidou I, Burchette J, et al. Mutations in the gene that encodes the F-actin binding protein anillin cause FSGS. *J Am Soc Nephrol.* (2014) 25:1991–2002. doi: 10.1681/ASN.2013090976
9. Endlich N, Schordan E, Cohen CD, Kretzler M, Lewko B, Welsch T, et al. Palladin is a dynamic actin-associated protein in podocytes. *Kidney Int.* (2009) 75:214–26. doi: 10.1038/ki.2008.486
10. Artelt N, Ludwig TA, Rogge H, Kavvadas P, Siegerist F, Blumenthal A, et al. The role of palladin in podocytes. *J Am Soc Nephrol.* (2018) 29:1662–78. doi: 10.1681/ASN.2017091039
11. Schordan S, Grisk O, Schordan E, Miehe B, Rumpel E, Endlich K, et al. OPN deficiency results in severe glomerulosclerosis in uninephrectomized mice. *Am J Physiol Renal Physiol.* (2013) 304:F1458–70. doi: 10.1152/ajprenal.00615.2012
12. Kindt F, Hammer E, Kemnitz S, Blumenthal A, Klemm P, Schlüter R, et al. A novel assay to assess the effect of pharmaceutical compounds on the differentiation of podocytes. *Br J Pharmacol.* (2017) 174:163–76. doi: 10.1111/bph.13667
13. Schindelin J, Arganda-Carreras I, Frise E, Kaynig V, Longair M, Pietzsch T, et al. Fiji: an open-source platform for biological-image analysis. *Nat Methods* (2012) 9:676–82. doi: 10.1038/nmeth.2019

14. Huff J. The Airyscan detector from ZEISS: confocal imaging with improved signal-to-noise ratio and super-resolution. *Nat Methods* (2015) 12:i–ii. doi: 10.1038/nmeth.f.388
15. Grgic I, Brooks CR, Hofmeister AF, Bijol V, Bonventre JV, Humphreys BD. Imaging of podocyte foot processes by fluorescence microscopy. *J Am Soc Nephrol.* (2012) 23:785–91. doi: 10.1681/ASN.2011100988
16. Höhne M, Ising C, Hagmann H, Völker LA, Brähler S, Schermer B, et al. Light microscopic visualization of podocyte ultrastructure demonstrates oscillating glomerular contractions. *Am J Pathol.* (2013) 182:332–8. doi: 10.1016/j.ajpath.2012.11.002
17. Putaala H, Soininen R, Kilpeläinen P, Wartiovaara J, Tryggvason K. The murine nephrin gene is specifically expressed inkidney, brain and pancreas: inactivation of the geneleads to massive proteinuria and neonatal death. *Hum Mol Genet.* (2001) 10:1–8. doi: 10.1093/hmg/10.1.1
18. Kestilä M, Lenkkeri U, Männikkö M, Lamerdin J, McCready P, Putaala H, et al. Positionally cloned gene for a novel glomerular protein—nephrin—is mutated in congenital nephrotic syndrome. *Mol Cell* (1998) 1:575–82.
19. Hassan H, Tian X, Inoue K, Chai N, Liu C, Soda K, et al. Essential role of X-Box binding protein-1 during endoplasmic reticulum stress in podocytes. *J Am Soc Nephrol.* (2016) 27:1055–65. doi: 10.1681/ASN.2015020191

Conflict of Interest Statement: PEMP (podocyte exact morphology measurement procedures) is registered for a patent. NE, KE, and FS are among the founders of the start-up NIPOKA which will commercialize PEMP.

The remaining authors declare that the research was conducted in the absence of any commercial or financial relationships that could be construed as a potential conflict of interest.

PLOS ONE

RESEARCH ARTICLE

The podocyte-specific knockout of palladin in mice with a 129 genetic background affects podocyte morphology and the expression of palladin interacting proteins

Nadine Artelt[1☯], Alina M. Ritter[1☯], Linda Leitermann[1], Felix Kliewe[1], Rabea Schlüter[2], Stefan Simm[3], Jens van den Brandt[4], Karlhans Endlich[1], Nicole Endlich[1]*

1 Institute for Anatomy and Cell Biology, University Medicine Greifswald, Greifswald, Germany, **2** Imaging Center of the Department of Biology, University of Greifswald, Greifswald, Germany, **3** Institute of Bioinformatics, University Medicine Greifswald, Greifswald, Germany, **4** Central Core and Research Facility of Laboratory Animals (ZSFV), University Medicine Greifswald, Greifswald, Germany

☯ These authors contributed equally to this work.
* nicole.endlich@uni-greifswald.de

OPEN ACCESS

Citation: Artelt N, Ritter AM, Leitermann L, Kliewe F, Schlüter R, Simm S, et al. (2021) The podocyte-specific knockout of palladin in mice with a 129 genetic background affects podocyte morphology and the expression of palladin interacting proteins. PLoS ONE 16(12): e0260878. https://doi.org/10.1371/journal.pone.0260878

Editor: Stuart E. Dryer, University of Houston, UNITED STATES

Received: June 16, 2021

Accepted: November 18, 2021

Published: December 8, 2021

Data Availability Statement: All relevant data are within the manuscript and its Supporting Information files.

Funding: This work was supported by a grant of the Federal Ministry of Education and Research (BMBF, grant 01GM1518B, STOP- FSGS) to Nicole Endlich. This work was generously supported by the Südmeyer fund for kidney and vascular research ('Südmeyer Stiftung für Nieren- und Gefäßforschung') and the Dr. Gerhard Büchtemann

Abstract

Proper and size selective blood filtration in the kidney depends on an intact morphology of podocyte foot processes. Effacement of interdigitating podocyte foot processes in the glomeruli causes a leaky filtration barrier resulting in proteinuria followed by the development of chronic kidney diseases. Since the function of the filtration barrier is depending on a proper actin cytoskeleton, we studied the role of the important actin-binding protein palladin for podocyte morphology. Podocyte-specific palladin knockout mice on a C57BL/6 genetic background (PodoPalldBL/6-/-) were back crossed to a 129 genetic background (PodoPalld129-/-) which is known to be more sensitive to kidney damage. Then we analyzed the morphological changes of glomeruli and podocytes as well as the expression of the palladin-binding partners Pdlim2, Lasp-1, Amotl1, ezrin and VASP in 6 and 12 months old mice. PodoPalld129-/- mice in 6 and 12 months showed a marked dilatation of the glomerular tuft and a reduced expression of the mesangial marker protein integrin α8 compared to controls of the same age. Furthermore, ultrastructural analysis showed significantly more podocytes with morphological deviations like an enlarged sub-podocyte space and regions with close contact to parietal epithelial cells. Moreover, PodoPalld129-/- of both age showed a severe effacement of podocyte foot processes, a significantly reduced expression of pLasp-1 and Pdlim2, and significantly reduced mRNA expression of *Pdlim2* and *VASP*, three palladin-interacting proteins. Taken together, the results show that palladin is essential for proper podocyte morphology in mice with a 129 background.

Introduction

More than 10% of the people worldwide are suffering from chronic kidney disease (CKD) and the tendency is still increasing [1]. In more than 75% of the diseased kidneys, a specific cell type in the filtration unit of the kidney, the podocyte, is damaged or lost [2].

fund, Hamburg, Germany. The funders had no role in study design, data collection and analysis, decision to publish, or preparation of the manuscript.

Competing interests: The authors have declared that no competing interests exist.

Podocytes are highly specialized and post mitotic epithelial cells that cover the outer aspect of the glomerular capillaries and are part of the filtration unit of the kidney. For proper and size selective blood filtration, a complex interdigitation of the podocyte foot processes and a slit membrane in between is indispensable. Many publications in the past have impressively shown that such a 3D morphology of the podocyte is highly dependent on the actin cytoskeleton and their specific actin-binding proteins such as α-actinin-4 [3–7]. The loss or mutation of this actin-bundling protein, for example, leads to foot process effacement and severe proteinuria [5]. Furthermore, it was shown that proteins, involved in the nucleation as well as polymerization of actin filaments are essential for podocytes and therefore for kidney function.

In the present study, we have examined the role of the actin-binding and nucleating protein palladin which is important for the organization and stability of the actin cytoskeleton in many cell types [8–10]. An ubiquitous knockout (KO) of palladin in mice is lethal *in utero* around E15.5 and embryos develop cranial neural tube closure defects [10, 11]. Palladin is a scaffold protein consisting of immunoglobulin domains and proline-rich regions that interact with different proteins [8, 12] like the vasodilator-stimulated phosphoprotein (VASP) [13], the LIM and SH3 protein 1 (Lasp-1) [14] as well as the actin-binding protein α-actinin-1 [15]. VASP has been shown to be a regulator of actin assembly [13] and Lasp-1 regulates the cytoskeleton dynamics and cell migration [16, 17]. Furthermore, palladin interacts with ezrin which cross links cortical actin filaments to the plasma membrane [12, 18]. Another palladin binding protein, Pdlim2, is expressed in podocyte foot processes [19, 20]. It has been shown to interact with α-actinin-4 as well as angiomotin-like 1 (Amotl1) and seems to be involved in the pathogenesis of glomerular disease due to a regulation of the actin dynamics [20]. Beside this, different palladin isoforms exist which are expressed in a tissue- and development-dependent way [8, 14, 21]. However, the function of the specific isoforms is mainly unknown.

Our group has shown that palladin is specifically expressed in podocytes and plays an important role for podocyte morphology and dynamics *in vivo* as well as *in vitro* [22]. Furthermore, we recently found that cultured podocytes with reduced palladin expression developed only a few actin fibers and were more susceptible for a disruption of actin filaments after the treatment with the actin polymerization inhibitor cytochalasin D [23]. Additionally, the expression of the podocyte-specific and actin-binding proteins synaptopodin and α-actinin-4 were significantly reduced after the knockdown of palladin in podocytes [23].

Studying the podocyte-specific palladin knockout in C57BL/6 mice (PodoPalldBL/6-/-), we observed changes of the morphology of the glomeruli. These PodoPalldBL/6-/- mice developed glomeruli with dilated capillaries at 6 months of age as well as a mild broadening (effacement) of the podocyte foot processes [23]. Since the effect of a specific knockout is highly dependent on the genetic background of the mice and C57BL/6 mice are known to be robust against kidney damage to some extent, we wanted to study the effect of palladin in mice with a 129 genetic background (PodoPalld129-/- mice), which is known to be more sensitive against kidney damage in many studies [24–26]. Therefore, we backcrossed PodoPalldBL/6-/- mice with the 129 strain and studied the morphological changes of the glomeruli and podocytes in 6 and 12 months old mice. Moreover, we analyzed the expression of the palladin-binding partners Pdlim2, Lasp-1, Amotl1, ezrin as well as VASP.

Materials and methods

Generation of PodoPalld129-/- mice

PodoPalldBL/6-/- mice were generated as described previously [23]. These mice have a C57BL/6 background and were backcrossed to the 129 background using 129S2/SvPasCrl

mice (Charles River Laboratories, Wilmington, MA, USA) and the *"speed congenics"* approach [27]. After 8x backcrossing, the new mouse line was established.

Podocyte-specific palladin knockout mice with 129 background (PodoPalld129-/-) and heterozygous Cre-recombinase expression were used for experiments. Mice without Cre-recombinase expression were used as controls (PodoPalld129+/+). Experiments were done with 6 and 12 months old male PodoPalld mice (at least n = 3 of each group). Genotyping of mice was performed with Phire® Animal Tissue Direct PCR Kit (Finnzymes/Thermo Fisher Scientific) in accordance to the manufacturer's instructions using primers shown in S1 Table.

All prerequisites of the German animal protection law were met and experiments were performed in accordance with the guidelines of the federal agencies in Mecklenburg-Western Pomerania (LALLF M-V). The responsible ethics committee within the LALLF M-V approved the experiments with mice. For kidney removal, mice were sacrificed by the use of barbiturate.

Histology staining

The samples were dehydrated and embedded into paraffin by standard procedures. Paraffin sections (4 μm) were performed on a Leica SM 2000R (Leica Microsystems). After deparaffinization, sections were rehydrated and PAS and H&E stainings were performed by standard procedures. Sections were mounted in Eukitt (Fluka/Sigma-Aldrich, St. Louis, MO, USA) and imaged with an Olympus BX50 microscope (Olympus Europe, Hamburg, Germany).

Immunofluorescence staining and immunohistochemistry of kidney sections

After deparaffinization, sections of mouse kidneys were rehydrated and unmasked in citrate buffer (0.1 M, pH 6.0) by heating for 5 min in a pressure cooker.

For immunofluorescence staining sections were blocked with blocking solution (2% FBS, 2% bovine serum fraction V, 0.2% fish gelatine in PBS) and incubated with the following primary antibodies overnight at 4˚C: guinea pig anti-nephrin (GP-N2, ProgenBiotechnik GmbH, Heidelberg, Germany; 1:100), rabbit anti-podocin(P-037-2, Sigma-Aldrich Corporation, St. Louis (USA); 1:250), rabbit anti-ezrin(HPA021616, Sigma-Aldrich; 1:250), anti-p-Lasp-1 (kindly provided by Dr. Elke Butt, Würzburg; 1:500), rabbit anti-integrin-α-8 (sc-25713, Santa Cruz, Dallas, TX, USA; 1:100), rabbit anti-Pdlim-2, (sc-292831, Santa Cruz; 1:50). Bound antibodies were visualized with Cy3-conjugated secondary antibodies (Jackson ImmunoResearch Laboratories, West Grove, PA, USA; 1:600). Sections were embedded in Mowiol (Carl Roth, Karlsruhe, Germany). Images were acquired using a Leica TCS SP5 confocal laser scanning microscope (Leica Microsystems, Wetzlar, Germany).

For immunohistochemistry (IHC), the Vectastain kit (SP-2001, Vector Laboratories, Burlingame, CA, USA) was used following manufacturer's instructions. Palladin was detected using rabbit anti-palladin (10853-1-AP, Proteintech Group, Manchester, UK; 1:850). Visualization was performed with DAB substrate kit (SK-4100; Vector Laboratories) followed by nuclear staining with hematoxylin and mounting in Eukitt (Sigma-Aldrich). In controls, PBS was used instead of primary antibody. Images were acquired using an Olympus BX50 microscope (Olympus Europe).

Isolation of mouse glomeruli

Glomeruli were isolated with magnetic Dynabeads as described previously [28].

RNA extraction and qRT-PCR analysis

Samples from glomeruli were processed in Tri-Reagent (Sigma-Aldrich) according to the manufacturer's instructions. For cDNA synthesis, 1 μg of isolated total RNA was reverse transcribed using the QuantiTect Reverse Transcription Kit (Qiagen, Hilden, Germany). Quantitative real-time PCR (qRT-PCR) was performed on a LightCycler® Nano (Roche Diagnostics GmbH, Mannheim, Germany) using iTaq Universal SYBR Green Supermix (Bio-Rad Laboratories GmbH, Hercules, CA, USA) and primers see S1 Table.

For qRT-PCR analysis we used the following number of mice per group: n = 5 of PodoPalld +/+ mice at 6 and 12 months of age, n = 6 and n = 7 of PodoPalld-/- mice at 6 and 12 months of age. Every control was compared to every PodoPalld-/- mouse for both age groups. The data were analyzed by standard methods [29] and the relative mRNA expression was calculated by normalizing values to the housekeeping gene *Rpl32*.

Asterisks indicate statistically significant differences ($p<0.05$) based on unpaired Student's t-test or Mann-Whitney U test between the *Rpl32* and targets of interest using GraphPad Prism 8 (GraphPad, La Jolla, CA, USA). For the tests, n replicates ($n\geq5$) were used and it was always checked for prerequisites such as normal distribution and similar variance between the measured groups.

Glomerular morphology analysis of mouse kidney

For transmission electron microscopy, kidneys were embedded in EPON 812 (SERVA, Heidelberg, Germany). Ultrathin sections were cut and contrasted with 5% uranyl acetate and lead citrate. All grids were examined with a LIBRA® 120 transmission electron microscope (Carl Zeiss Microscopy, Jena, Germany).

Scanning electron microscopy was performed according to Artelt *et al.* [30].

Furthermore, the presence of glomerular abnormalities was investigated more precisely using Richardson's (Azur II/ Methylene blue) stained semithin sections of mouse kidneys. Glomeruli were categorized into (i) glomeruli with normal morphology, (ii) dilated capillaries and (iii) affected podocytes (podocytes with cyst and enlarged sub-podocyte space). The presence of dilated capillaries was verified by quantitative analysis of the capillary area per glomerulus on semithin sections.

We analyzed at least n = 3 mice of each group with a total of at least 30 glomeruli. Asterisks indicate statistically significant differences ($p<0.05$) based on two-way ANOVA analysis with FDR correction using GraphPad Prism 8.

Results

Confirmation of the podocyte-specific palladin knockout

To confirm that the backcrossed PodoPalld129-/- mice show a podocyte-specific knockout for palladin, we analyzed the animals by immunohistochemistry (IHC) and qRT-PCR. The IHC staining of PodoPalld129-/- mice revealed that the podocytes were palladin-negative at the age of 6 as well as of 12 months in contrast to the controls (S1A Fig). A faint signal for palladin (6 months: 0.26 ±0.14, 12 months: 0.19±0.05; mean±SD) was detected by qRT-PCR of isolated glomeruli which is due to a slight contamination with small vessels that still express palladin as shown in S1 Fig.

PodoPalld129-/- mice show dilated capillaries as well as a reduced number of mesangial cells

We studied the glomerular morphology of two groups of mice, one group with an age of 6 months and the other with an age of 12 months by histological and ultrastructural analysis. All

glomeruli of the PodoPalld129-/- mice developed severe dilatation of the capillaries as shown by a Periodic Acid Schiff (PAS) and Hematoxylin and Eosin (H&E) staining (Fig 1A and S2 Fig). We found that 38.1±9.4% (PodoPalld129-/-) vs. 16.5±5.2% (control; mean±SD, $p<0.01$) of the glomeruli at 6 month and 38.0±5.6% (PodoPalld129-/-) vs. 31.9±1.8% (control; mean ±SD) at 12 months developed a dilatation of their capillaries (n = 3 animals and >60 analyzed glomeruli per group, Fig 1B). Quantitative analysis of the capillary area per glomerular area underlined that the capillaries of PodoPalld129-/- glomeruli were significantly enlarged (6 months: 0.46±0.06, $p<0.05$; 12 months: 0.50±0.07, $p<0.05$; mean±SD) compared to the control glomeruli (6 months: 0.36±0.02, 12 months: 0.40±0.03; mean±SD) (n≥3 animals and >30 glomeruli per group, Fig 1B). Since the dilatation of the glomerular tuft could be caused by a lower number of mesangial cells, we stained for the specific integrin α8 that is expressed in mesangial cells. Interestingly, we observed a marked reduction of the integrin α8 signal in 6 as well as in 12 months old PodoPalld129-/-mice compared to corresponding controls (Fig 1C) suggesting that palladin might influence the development or the survival of mesangial cells. The reduction of the Itga8 expression in PodoPalld129-/-mice was verified by Western blot (Fig 1D).

Podocytes of PodoPalld129-/- mice develop morphological abnormalities

To study the morphology of PodoPalld129-/- glomeruli in 6 and 12 months in more detail, we used Richardson's stained semithin sections as well as ultrathin sections for the analysis by the transmission electron microscopy (TEM). Hereby, we found an enlargement of the so-called sub-podocyte space in animals with an age of 6 and 12 months, shown in Fig 2A and 2B. Furthermore, we identified several podocytes with autophagosomes and laminar bodies, respectively (Fig 2C). Moreover, we observed regions with a close contact of podocytes to parietal epithelial cells in both age groups of PodoPalld129-/- mice (Fig 2D). Quantitative analysis of PodoPalld129-/- glomeruli in comparison to the controls showed significantly more morphological alterations e.g. an enlarged sub-podocyte space, with an age of 6 months (39.9±4.1% vs. 6.3±2.1%; mean±SD, $p<0.01$) as well as of 12 months (45.4±6.8% vs. 23.2±18.9%; mean±SD, $p<0.05$ (n = 3 animals and >60 analyzed glomeruli per group, Fig 2E). Therefore, PodoPalld129-/- mice had correspondingly significantly fewer glomeruli with normal morphology than controls at 6 months (22.0±6.0% vs. 77.2±4.5%; mean±SD, $p<0.05$) as well as 12 months of age (16.6±6.7% vs. 44.9±20.6%; mean±SD, $p<0.05$) (n = 3 animals and >60 analyzed glomeruli per group, Fig 2E).

The loss of palladin results in podocyte foot process effacement

Since PodoPalld129-/- mice developed morphological abnormalities we studied the expression of slit membrane proteins and foot process morphology in detail. Immunohistological staining showed that the slit membrane protein nephrin was significantly reduced in 6 as well as in 12 months old PodoPalld129-/-mice compared to the controls (Fig 3A), whereas expression of the nephrin mRNA was unchanged (6 months: 1.05±0.27, 12 months: 0.98±0.26; mean±SD) (S3 Fig). The same results were received for the slit membrane protein podocin (mRNA level 6 months: 1.09±0.32, 12 months: 1.07±0.37; mean±SD) (S3 Fig). A severe effacement of the podocyte foot processes was demonstrated by ultrastructural analysis using transmission electron microscopy (Fig 3B) and scanning electron microscopy (SEM, Fig 3C). Furthermore, quantification of the foot process area confirmed an increased podocyte foot process effacement in 6 months as wells as 12 months old PodoPalld129-/- mice compared to the corresponding controls (Fig 3D). Podocyte-specific loss of palladin does not result in proteinuria or albuminuria measured by dip stick and SDS electrophoresis (S5 Fig).

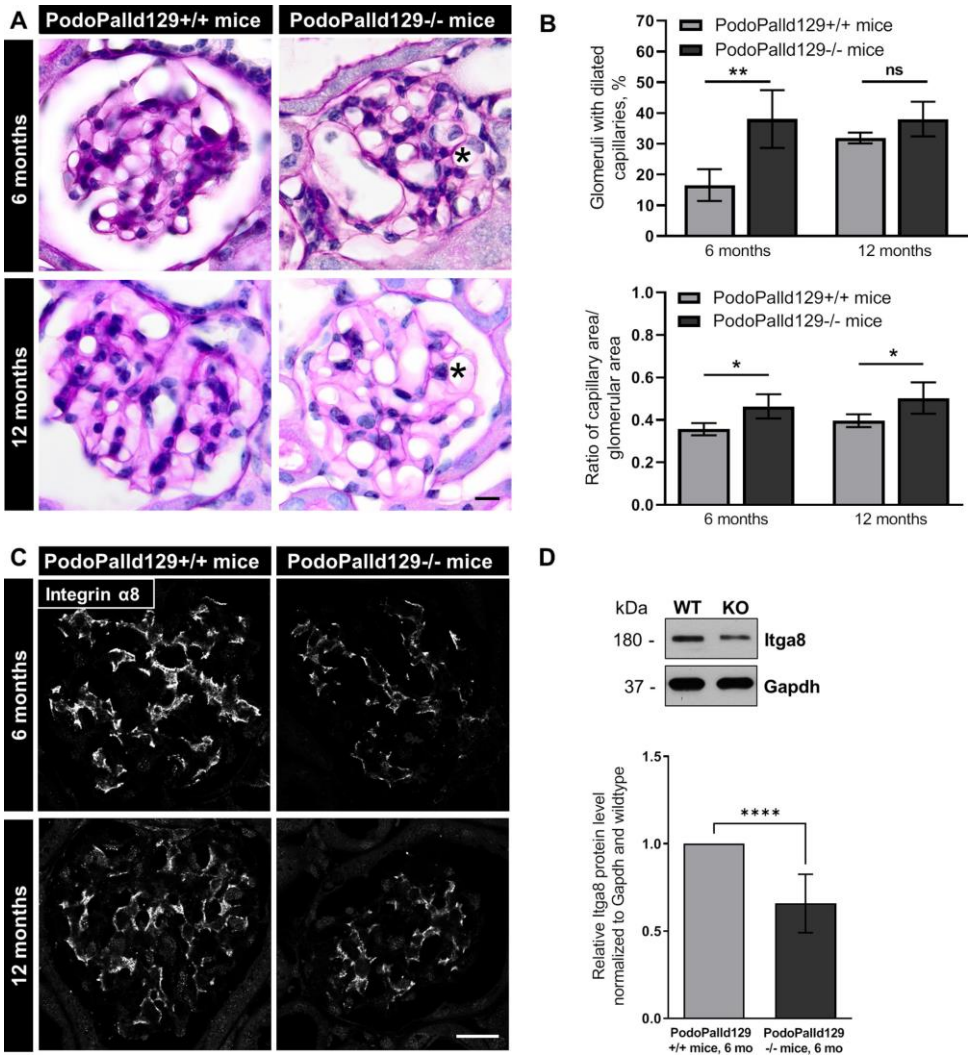

Fig 1. Glomeruli of PodoPalld129-/- mice have dilated capillaries and show a reduced expression of integrin α8. (A) The periodic acid staining of paraffin kidney sections revealed dilated capillaries in 6 and 12 months old PodoPalld129-/- mice (asterisks). Scale bar represents 10 μm. (B) Quantitative analysis confirmed that PodoPalld129-/- mice of both age groups have significantly more glomeruli with dilated capillaries than controls of the same age. (C) Immunofluorescence staining of kidney sections showed a marked reduction of integrin α8 expression in PodoPalld129-/- glomeruli. Scale bar represents 20 μm. (D) Western blot quantification of Itga8 showed a significant decrease in 6 months old PodoPalld129-/- glomeruli (KO) compared to the control (WT; 6 months old PodoPalld129+/+ glomeruli protein lysates). Data are presented as means ± SD; * $p<0.05$; ** $p<0.01$; **** $p<0.001$; ns, not significant; two-way ANOVA with FDR correction (B) or unpaired Student's t-test (D).

https://doi.org/10.1371/journal.pone.0260878.g001

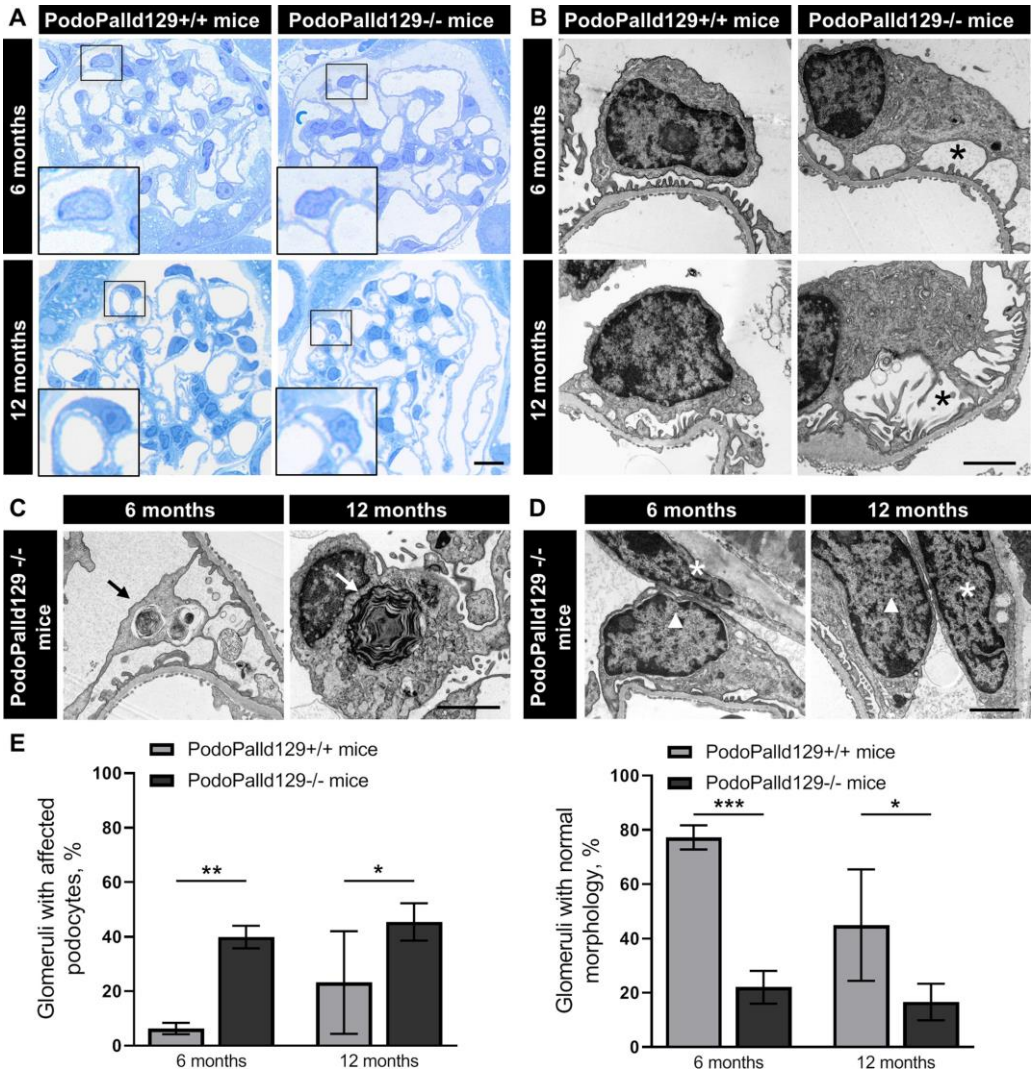

Fig 2. Podocytes of PodoPalld129-/- mice show morphological abnormalities. (A) In Richardson's stained semithin sections of PodoPalld129-/- mice we have found podocytes with enlarged subpodocyte space compared with controls as illustrated in the higher magnifications. Scale bar represents 10 μm. (B) TEM images show podocytes with enlarged subpodocyte space in both age groups of PodoPalld129-/- mice (asterisks). (C, D) Podocytes with autophagosomes/laminar bodies (arrows) and contacts between parietal epithelial cells (asterisks) and podocytes (arrowhead) were found in TEM images of both age groups in PodPalld129-/- mice. Scale bars represent 2 μm. (E) PodoPalld129-/- mice had significantly more glomeruli with affected podocytes and correspondingly significantly fewer glomeruli without abnormalities than controls of the same age (mean±SD, * $p<0.05$, ** $p<0.01$ and *** $p<0.001$; two-way ANOVA with FDR correction).

https://doi.org/10.1371/journal.pone.0260878.g002

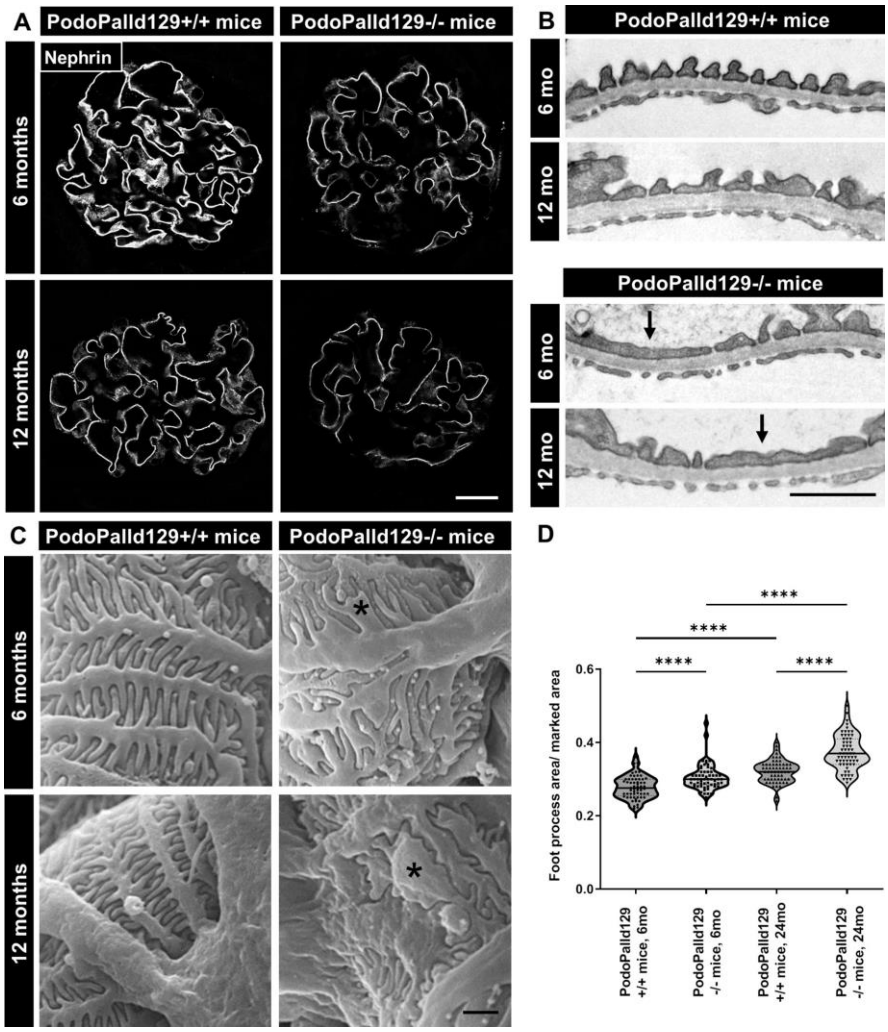

Fig 3. PodoPalld129-/- mice have effaced podocyte foot processes. (A) Immunofluorescence staining of kidney sections shows a reduced expression of the slit membrane protein nephrin in PodoPalld129-/- mice compared with corresponding controls. Scale bar represents 20 μm. (B) Transmission electron micrographs (arrows) and (C) scanning electron micrographs (asterisks) revealed strongly effaced podocyte foot processes in PodoPalld129-/- mice. Scale bars represents 1 μm. (D) Quantification of foot process area confirmed the increased podocyte foot process effacement in 6 months as wells as 12 months old PodoPalld129-/- mice compared with corresponding controls. Data are represented as violin plot (**** $p<0.0001$; two-way ANOVA with FDR correction).

https://doi.org/10.1371/journal.pone.0260878.g003

Palladin knockout affects the expression of actin-binding proteins

Since podocyte morphology is highly dependent on the actin-cytoskeleton with their actin-binding proteins, we analyzed the role of palladin on the expression of essential actin- and

palladin-binding proteins like Pdlim2, VASP, Lasp-1, ezrin and Amotl1, which were all expressed in podocytes. After the immunofluorescence staining of kidney sections, we found that Pdlim2 and phosphorylated Lasp-1 (pLasp-1) was markedly reduced in PodoPalld129-/- mice at the age of 6 as well as of 12 months compared with the controls (Fig 4A). In contrast, the protein expression of ezrin was unchanged (Fig 4A). Different antibodies against Lasp-1 and VASP showed unfortunately no reactivity on mouse tissue. mRNA expression analysis showed that *Pdlim2* was also significantly reduced in the glomeruli (6 months: 0.82±0.20, $p<0.001$; mean±SD), whereas *Ezrin* was unchanged (6 months: 1.03±0.31; mean±SD) (Fig 4B). This was also confirmed by Western blot quantification (Fig 4C). qRT-PCR analysis further showed a significant down-regulation of *VASP* mRNA level (6 months: 0.71±0.41, $p<0.01$; 12 months: 0.78±0.28; $p<0.001$; mean±SD) and an upregulation of *Amotl1* mRNA level (6 months: 1.51±0.47, $p<0.001$; 12 months: 1.32±0.57, $p<0.01$; mean±SD) compared to controls with the same age (S4 Fig).

Discussion

Palladin, an essential actin-binding and regulating protein, is ubiquitously expressed in mammals [8, 12]. Recently, our group has shown that palladin is specifically expressed in podocytes, a post mitotic cell type in the kidney [22] where it plays an important role in cross-linking and stabilization of actin filaments [8, 31]. Additionally, we demonstrated that palladin is essential for a proper 3D morphology of podocytes as well as for the glomerular tuft formation *in vivo*, especially after the challenge of the mice with nephrotoxic serum (NTS), which is a well-established kidney disease model [23, 32].

It is well known that the genetic background of the mouse strain has an important influence on the severeness and development of kidney disease. As it was nicely shown by Steppan and colleagues, mouse strains have distinct vascular properties [33]. They have found that the blood pressure seems to be similar in 129S and C57BL/6 strains, however there are significant differences in vascular properties which might influence the severeness and onset of kidney diseases. Therefore, it is important to study the role of proteins in different and good characterized mouse strains.

Here we studied the influence of palladin not only in the mainly used C57BL/6 mice strain, which is often described to be robust against kidney damage, but also in the often more sensitive 129 genetic mouse strain [24–26]. For this purpose, we backcrossed the palladin knockout mice to the 129 background and analyzed the animals at an age of 6 months and 12 months. We have found that PodoPalld129-/- mice were more affected by the palladin knockout compared with PodoPalldBL/6-/-mice. In 6 month old knockout mice with a C57BL/6 background, approximately 20% of glomeruli showed dilated capillaries [23]. In contrast, glomeruli of 6 months old PodoPalld129-/-mice showed a significant increased dilatation of the glomerular tuft (38±9.4%) compared to the control mice (16.5±5.2%; mean±SD, $p<0.01$) at the same age. Interestingly, the number of glomeruli with dilated capillaries did not increase further in 12 months old PodoPalld129-/- mice, indicating that the glomerular phenotype developed already during the first 6 months. This analysis underlines the importance of the genetic background of animals with a specific knockout because it severely influences the phenotype.

To identify the reason for such a dilatation in PodoPalld129-/- mice, we investigated the presence of mesangial cells. Mesangial cells are contractile cells and play a key role in capillary loop formation [34]. Since there is an interaction and cross-talk between mesangial cells, endothelial cells and podocytes [34], we examined whether the palladin knockout in podocytes also has an indirect effect on mesangial cells. To investigate this we stained kidney sections with an antibody specific for mesangial cells against integrinα8 [35] and found a significant

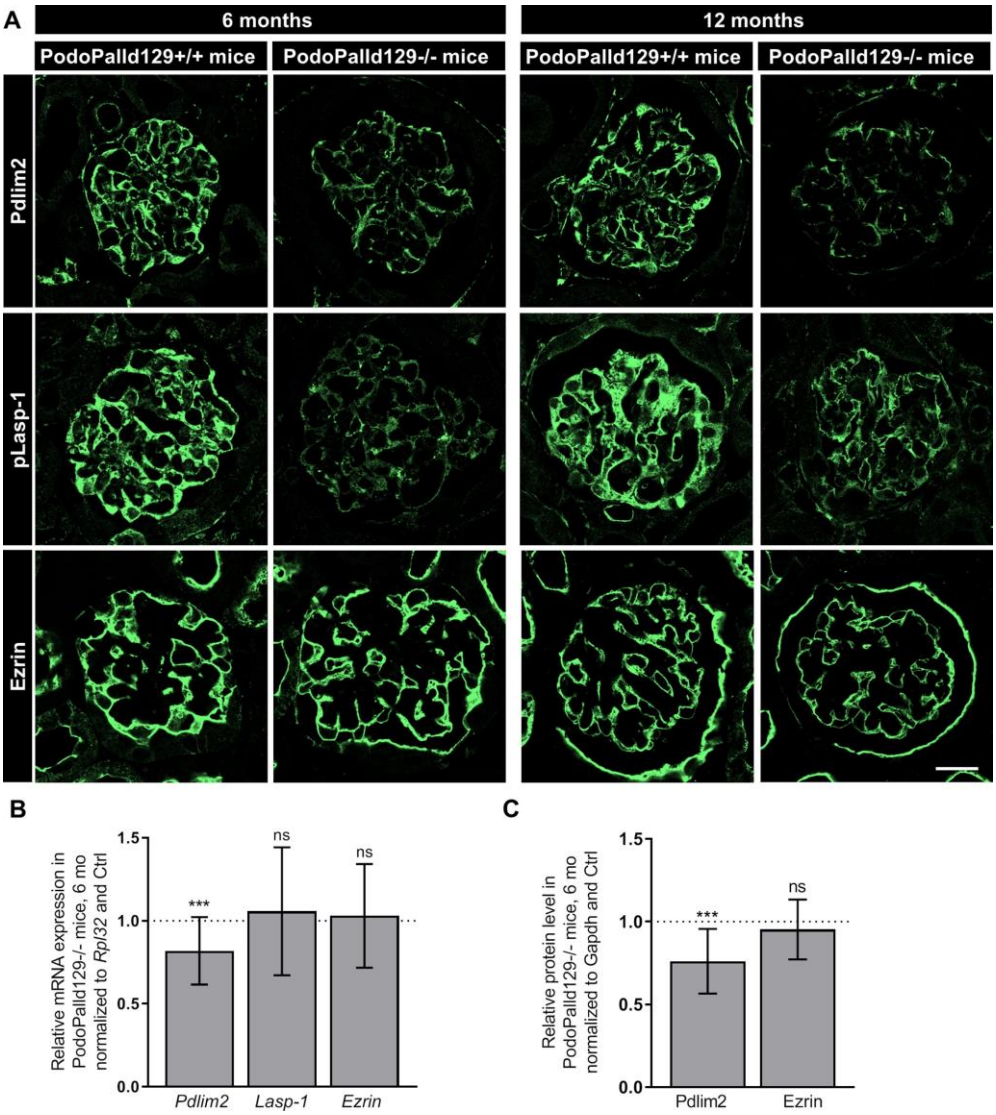

Fig 4. Analysis of palladin interacting proteins in PodoPalld129 mice. (A) Immunofluorescence stainings of kidney sections show a reduced expression of Pdlim2 and pLasp-1 in PodoPalld129-/- mice compared with corresponding controls. No difference was found for ezrin. Scale bar represents 20 μm. (B) A significant downregulation of *Pdlim2* mRNA in 6 months old PodoPalld129-/- glomeruli was found by qRT-PCR. *Lasp-1* and *Ezrin* were not significantly changed. (C) Relative protein level in 6 months old PodoPalld129-/- glomeruli normalized to Gapdh and protein lysates of PodoPalld129+/+ glomeruli. Data are presented as means±SD; *** $p<0.001$; ns, not significant; unpaired Student's t-test.

https://doi.org/10.1371/journal.pone.0260878.g004

downregulation of the protein. This could also be observed by loss of mesangial cells in early stages of glomerulonephritis/-sclerosis when mesangiolysis and capillary expansion occurred [36, 37]. Since we found only a faint staining for this specific integrin in the glomeruli of PodoPalld129-/- mice in contrast to the control mice at the same age, we hypothesized that here the number of mesangial cells is reduced. Whether this is due to a developmental failure or caused by the loss of mesangial cells after birth is still unknown.

Beside a dilatation of the glomerular tuft, we found that the majority of PodoPalld129-/- podocytes developed an enlarged sub-podocyte space as well as cysts compared to the controls of the same strain and to podocytes of the PodoPalldBL/6-/- mice [23]. Ultrastructural analysis of the foot processes by scanning and transmission electron microscopy revealed that nearby 50% of the analyzed PodoPalld129-/- podocytes in mice with an age of 12 months developed such a severe phenotype. Moreover, this phenotype was already described by Kriz and colleagues in a variety of models [38, 39]. Based on descriptions in different podocyte-related diseases [40–42], our results lead to two assumptions. First, this phenotype could be caused by an imbalanced growth of the glomerular tuft due to a low number of mesangial cells and/or by podocyte hypertrophy to compensate lost podocytes which might be characteristic for this specific strain. Second, it could be that difference is vascular stiffness observed by Steppan and colleagues [33] leads to a higher risk of developing glomerular hypertension, especially already at a young age.

Furthermore, PodoPalld129-/- mice at 12 months of age showed more effaced foot processes compared to 6 months old mice. This finding is in nice agreement with the quantification of podocyte foot process morphology by super resolution microscopy as already described [30]. Here we could show that 6 and 12 months old PodoPalld129-/- mice possess a significant reduction of the filtration slit density (FSD) resulting insignificantly more effaced podocyte foot processes compared to the littermates [30]. In addition, in this study we could show that protein expressions of the slit diaphragm proteins nephrin and podocin were significantly downregulated in PodoPalld129-/- mice compared to corresponding controls.

Beside the morphological findings, we observed autophagosomes in PodoPalld129-/- podocytes which is a hallmark of autophagy, a self-repair mechanism of post mitotic cells [43]. Interestingly, patients suffering from IgA nephropathy and membranous nephropathy, both podocyte-related kidney diseases, showed also an increase of autophagosomes in podocytes [44, 45].

Moreover, ultrastructural analysis revealed an increased number of contacts between podocytes and parietal epithelial cells (PECs) in PodoPalld129-/- glomeruli. This is of specific interest since it is known that contacts between podocytes and PECs trigger the formation of tuft adhesions that are first committed lesions for focal segmental glomerulosclerosis. [46–48].

The podocyte foot process morphology is highly dependent on an intact actin cytoskeleton. Therefore, we studied the influence of palladin on the actin cytoskeleton in these specific knockout mice. Since it is described that palladin has specific binding-sites for proteins which are involved in actin dynamics and stability like Lasp-1 [14], Pdlim2 [19], ezrin [12], and VASP [13], we investigated the effect of the palladin knockout on the expression of these proteins. Although palladin is known to recruit Lasp-1to actin stress fibres and that the palladin knockdown in HeLa cells resulted in a reduction of Lasp-1 [14, 49], we have found that the *Lasp-1* mRNA expression was unchanged in PodoPalld129-/- podocytes. However, the phosphorylation of Lasp-1 was significantly reduced. This might influence the stability of the podocyte foot processes, since it was already shown that phosphorylation of Lasp-1 reduces the binding to F-actin *in vitro* [16, 50].

Furthermore, we have detected a significant down-regulation of Pdlim2 in podocytes of PodoPalld129-/- mice. Pdlim2 was already shown to be essential for the stability of the actin

cytoskeleton in cultured podocytes as well as was regulated in patients suffering from glomerulopathies [20]. Interestingly, the Pdlim2-interacting partner Amotl1 [20], a protein which regulates the actin dynamic [51], was significantly up-regulated in PodoPalld129-/-glomeruli. Probably, Amotl1 is able to compensate the reduced Pdlim2 expression.

Another important actin-binding protein, VASP, which also regulates actin dynamics, was significantly down-regulated in 6 and 12 months old PodoPalld129-/- mice, indicating that palladin directly influence this protein via the binding site. In contrast, we observed no difference in the expression of ezrin, an actin-binding and plasma membrane cross-linking protein [52], between control and PodoPalld129-/- mice.

Taken together, this study demonstrates that palladin has an impact on the expression of the interacting proteins Pdlim2, pLasp and VASP and is important for capillary tuft formation and podocyte morphology.

Supporting information

S1 Fig. Generation of PodoPalld129-/- mice and confirmation of the podocyte-specific KO of palladin. (A) The specific palladin KO was confirmed by immunohistochemistry staining of paraffin kidney sections. PodoPalld129+/+ mice exhibit strong palladin-expressing podocytes (arrow). In contrast, there is no palladin signal (arrowhead) in PodoPalld129-/- podocytes. Scale bar represents 10 μm. (B) In addition, the palladin KO was verified by qRT-PCR (mean±SD, $^{***}p<0.001$; 6 months: Mann-Whitney U test, 12 months: unpaired Student's t-test).
(TIF)

S2 Fig. Glomeruli of PodoPalld129-/- mice have dilated capillaries. The hematoxylin and eosin staining of paraffin kidney sections showed dilated capillaries in 6 and 12 months old PodoPalld129-/- mice (asterisks). Scale bar represents 10 μm.
(TIF)

S3 Fig. Analysis of slit membrane proteins of PodoPalld129 mouse glomeruli. (A) Quantitative analysis of nephrin mRNA levels in isolated glomeruli showed no significant difference between PodoPalld129-/- mice and controls (mean±SD; unpaired Student's t-test). (B) Immunofluorescence staining of kidney sections reveal a slightly decreased expression of the slit membrane protein podocin in PodoPalld129-/- mice compared with corresponding controls. Scale bar represents 20 μm. (C) However, we found no significant difference of podocin mRNA in isolated glomeruli of PodoPalld129-/- and PodoPalld129+/+ mice (mean±SD; 6 months: Mann-Whitney U test, 12 months: unpaired Student's t-test).
(TIF)

S4 Fig. Quantitative analysis of mRNA level of palladin-interacting proteins. A significant downregulation of *Vasp* mRNA and upregulation of *Amotl1* mRNA in PodoPalld129-/- glomeruli was found by qRT-PCR. Data are presented as means ± SD; ** $p<0.01$; *** $p<0.001$; unpaired Student's t-test.
(TIF)

S5 Fig. Quantitative analysis of urine of PodoPalld129+/+ and PodoPalld129-/- mice. Equal volume of sterile urine from 6- and 12-months old PodoPalld129+/+ and PodoPalld129-/- mice were separated by SDS-Page and were subsequently stained using CBB (Coomassie Brilliant Blue). BSA was used as a charge control (lane 2). No albumin band is seen (dotted outline), in 6 months old PodoPalld129-/- (lane 4–6) as well as in 12 months old PodoPalld129-/- (lane 8–10) indicating no increased proteinuria in the PodoPalld129-/- mice. The

major urinary proteins (MUPs) showed a strong signal between 15 kDa and 20 kDa.
(TIF)

S1 Table. Primer for RT-PCR and qRT-PCR.
(DOCX)

Acknowledgments

The authors thank Mandy Weise, Claudia Weber, Antje Blumenthal and Stefan Bock for technical assistance. The 2.5P-Cre mice and primers for genotyping PodoPalld129 mice were kindly provided by Prof. Marcus J. Moeller (Department of Internal Medicine II—Nephrology and Clinical Immunology, Rheinisch-Westfälische Technische Hochschule (RWTH) Aachen University Hospital, Aachen, Germany).

Author Contributions

Conceptualization: Nadine Artelt, Karlhans Endlich, Nicole Endlich.

Formal analysis: Nadine Artelt.

Investigation: Nadine Artelt, Alina M. Ritter, Linda Leitermann, Felix Kliewe, Rabea Schlüter.

Project administration: Nadine Artelt.

Resources: Jens van den Brandt.

Software: Stefan Simm.

Supervision: Nadine Artelt, Karlhans Endlich, Nicole Endlich.

Validation: Nadine Artelt, Felix Kliewe, Stefan Simm.

Visualization: Nadine Artelt, Alina M. Ritter, Linda Leitermann, Felix Kliewe.

Writing – original draft: Nadine Artelt, Alina M. Ritter, Nicole Endlich.

Writing – review & editing: Nadine Artelt, Rabea Schlüter, Karlhans Endlich, Nicole Endlich.

References

1. Bikbov B, Purcell CA, Levey AS, Smith M, Abdoli A, Abebe M, et al. Global, regional, and national burden of chronic kidney disease, 1990–2017: a systematic analysis for the Global Burden of Disease Study 2017. The Lancet. 2020; 395:709–33. https://doi.org/10.1016/S0140-6736(20)30045-3 PMID: 32061315
2. Wiggins RC. The spectrum of podocytopathies: a unifying view of glomerular diseases. Kidney Int. 2007; 71:1205–14. Epub 2007/04/04. https://doi.org/10.1038/sj.ki.5002222 PMID: 17410103.
3. Kaplan JM, Kim SH, North KN, Rennke H, Correia LA, Tong HQ, et al. Mutations in ACTN4, encoding alpha-actinin-4, cause familial focal segmental glomerulosclerosis. Nat Genet. 2000; 24:251–6. https://doi.org/10.1038/73456 PMID: 10700177.
4. Michaud J-L. Focal and Segmental Glomerulosclerosis in Mice with Podocyte-Specific Expression of Mutant -Actinin-4. Journal of the American Society of Nephrology. 2003; 14:1200–11. https://doi.org/10.1097/01.asn.0000059864.88610.5e PMID: 12707390
5. Kos CH, Le TC, Sinha S, Henderson JM, Kim SH, Sugimoto H, et al. Mice deficient in α-actinin-4 have severe glomerular disease. J Clin Invest. 2003; 111:1683–90. https://doi.org/10.1172/JCI17988 PMID: 12782671
6. Perico L, Conti S, Benigni A, Remuzzi G. Podocyte-actin dynamics in health and disease. Nat Rev Nephrol. 2016; 12:692–710. Epub 2016/08/30. https://doi.org/10.1038/nrneph.2016.127 PMID: 27573725.
7. Garg P. A Review of Podocyte Biology. Am J Nephrol. 2018; 47 Suppl 1:3–13. Epub 2018/05/31. https://doi.org/10.1159/000481633 PMID: 29852492.

8. Parast MM, Otey CA. Characterization of Palladin, a Novel Protein Localized to Stress Fibers and Cell Adhesions. J Cell Biol. 2000; 150:643–56. https://doi.org/10.1083/jcb.150.3.643 PMID: 10931874

9. Beck MR, Dixon RDS, Goicoechea SM, Murphy GS, Brungardt JG, Beam MT, et al. Structure and function of palladin's actin binding domain. J Mol Biol. 2013; 425:3325–37. https://doi.org/10.1016/j.jmb.2013.06.016 PMID: 23806659.

10. Luo H, Liu X, Wang F, Huang Q, Shen S, Wang L, et al. Disruption of palladin results in neural tube closure defects in mice. Molecular and Cellular Neuroscience. 2005; 29:507–15. https://doi.org/10.1016/j.mcn.2004.12.002 PMID: 15950489

11. Tan J, Chen X-J, Shen C-L, Zhang H-X, Tang L-Y, Lu S-Y, et al. Lacking of palladin leads to multiple cellular events changes which contribute to NTD. Neural Dev. 2017; 12:4. Epub 2017/03/24. https://doi.org/10.1186/s13064-017-0081-6 PMID: 28340616.

12. Mykkänen O-M, Grönholm M, Rönty M, Lalowski M, Salmikangas P, Suila H, et al. Characterization of Human Palladin, a Microfilament-associated Protein. MBoC. 2001; 12:3060–73. https://doi.org/10.1091/mbc.12.10.3060 PMID: 11598191

13. Boukhelifa M, Parast MM, Bear JE, Gertler FB, Otey CA. Palladin is a novel binding partner for Ena/VASP family members. Cell Motil Cytoskeleton. 2004; 58:17–29. https://doi.org/10.1002/cm.10173 PMID: 14983521

14. Rachlin AS, Otey CA. Identification of palladin isoforms and characterization of an isoform-specific interaction between Lasp-1 and palladin. J Cell Sci. 2006; 119:995–1004. https://doi.org/10.1242/jcs.02825 PMID: 16492705.

15. Rönty M, Taivainen A, Moza M, Otey CA, Carpén O. Molecular analysis of the interaction between palladin and α-actinin. FEBS Letters. 2004; 566:30–4. https://doi.org/10.1016/j.febslet.2004.04.006 PMID: 15147863

16. Chew CS, Chen X, Parente JA, Tarrer S, Okamoto C, Qin H-Y. Lasp-1 binds to non-muscle F-actin in vitro and is localized within multiple sites of dynamic actin assembly in vivo. J Cell Sci. 2002; 115:4787–99. https://doi.org/10.1242/jcs.00174 PMID: 12432067.

17. Butt E, Gambaryan S, Göttfert N, Galler A, Marcus K, Meyer HE. Actin binding of human LIM and SH3 protein is regulated by cGMP- and cAMP-dependent protein kinase phosphorylation on serine 146. J Biol Chem. 2003; 278:15601–7. https://doi.org/10.1074/jbc.M209009200 PMID: 12571245.

18. Kawaguchi K, Yoshida S, Hatano R, Asano S. Pathophysiological Roles of Ezrin/Radixin/Moesin Proteins. Biol Pharm Bull. 2017; 40:381–90. https://doi.org/10.1248/bpb.b16-01011 PMID: 28381792.

19. Maeda M, Asano E, Ito D, Ito S, Hasegawa Y, Hamaguchi M, et al. Characterization of interaction between CLP36 and palladin. FEBS J. 2009; 276:2775–85. https://doi.org/10.1111/j.1742-4658.2009.07001.x PMID: 19366376.

20. Sistani L, Dunér F, Udumala S, Hultenby K, Uhlen M, Betsholtz C, et al. Pdlim2 is a novel actin-regulating protein of podocyte foot processes. Kidney Int. 2011; 80:1045–54. https://doi.org/10.1038/ki.2011.231 PMID: 21814175.

21. Wang H-V, Moser M. Comparative expression analysis of the murine palladin isoforms. Dev Dyn. 2008; 237:3342–51. https://doi.org/10.1002/dvdy.21755 PMID: 18924229.

22. Endlich N, Schordan E, Cohen CD, Kretzler M, Lewko B, Welsch T, et al. Palladin is a dynamic actin-associated protein in podocytes. Kidney Int. 2009; 75:214–26. https://doi.org/10.1038/ki.2008.486 PMID: 19116644.

23. Artelt N, Ludwig TA, Rogge H, Kavvadas P, Siegerist F, Blumenthal A, et al. The Role of Palladin in Podocytes. J Am Soc Nephrol. 2018; 29:1662–78. https://doi.org/10.1681/ASN.2017091039 PMID: 29720549.

24. Ma L-J, Fogo AB. Model of robust induction of glomerulosclerosis in mice: importance of genetic background. Kidney Int. 2003; 64:350–5. https://doi.org/10.1046/j.1523-1755.2003.00058.x PMID: 12787428.

25. Qi Z, Fujita H, Jin J, Davis LS, Wang Y, Fogo AB, et al. Characterization of Susceptibility of Inbred Mouse Strains to Diabetic Nephropathy. Diabetes. 2005; 54:2628–37. https://doi.org/10.2337/diabetes.54.9.2628 PMID: 16123351

26. Ishola DA, van der Giezen DM, Hahnel B, Goldschmeding R, Kriz W, Koomans HA, et al. In mice, proteinuria and renal inflammatory responses to albumin overload are strain-dependent. Nephrol Dial Transplant. 2006; 21:591–7. https://doi.org/10.1093/ndt/gfi303 PMID: 16326737.

27. Wong GT. Speed congenics: applications for transgenic and knock-out mouse strains. Neuropeptides. 2002; 36:230–6. https://doi.org/10.1054/npep.2002.0905 PMID: 12359513.

28. Kindt F, Hammer E, Kemnitz S, Blumenthal A, Klemm P, Schlüter R, et al. A novel assay to assess the effect of pharmaceutical compounds on the differentiation of podocytes. Br J Pharmacol. 2017; 174:163–76. https://doi.org/10.1111/bph.13667 PMID: 27858997.

29. Livak KJ, Schmittgen TD. Analysis of relative gene expression data using real-time quantitative PCR and the 2(-Delta C(T)) Method. Methods. 2001; 25:402–8. https://doi.org/10.1006/meth.2001.1262 PMID: 11846609.

30. Artelt N, Siegerist F, Ritter AM, Grisk O, Schlüter R, Endlich K, et al. Comparative Analysis of Podocyte Foot Process Morphology in Three Species by 3D Super-Resolution Microscopy. Front Med (Lausanne). 2018; 5:292. https://doi.org/10.3389/fmed.2018.00292 PMID: 30425988.

31. Dixon RDS, Arneman DK, Rachlin AS, Sundaresan NR, Costello MJ, Campbell SL, et al. Palladin Is an Actin Cross-linking Protein That Uses Immunoglobulin-like Domains to Bind Filamentous Actin. J Biol Chem. 2008; 283:6222–31. https://doi.org/10.1074/jbc.M707694200 PMID: 18180288

32. Ougaard MKE, Kvist PH, Jensen HE, Hess C, Rune I, Søndergaard H. Murine Nephrotoxic Nephritis as a Model of Chronic Kidney Disease. Int J Nephrol. 2018; 2018:8424502. Epub 2018/03/05. https://doi.org/10.1155/2018/8424502 PMID: 29692933.

33. Steppan J, Jandu S, Wang H, Kang S, Savage W, Narayanan R, et al. Commonly used mouse strains have distinct vascular properties. Hypertens Res. 2020; 43:1175–81. Epub 2020/05/14. https://doi.org/10.1038/s41440-020-0467-4 PMID: 32409775.

34. Schlöndorff D, Banas B. The mesangial cell revisited: no cell is an island. J Am Soc Nephrol. 2009; 20:1179–87. https://doi.org/10.1681/ASN.2008050549 PMID: 19470685.

35. Hartner A, Schöcklmann H, Pröls F, Müller U, Sterzel RB. Alpha8 integrin in glomerular mesangial cells and in experimental glomerulonephritis. Kidney Int. 1999; 56:1468–80. https://doi.org/10.1046/j.1523-1755.1999.00662.x PMID: 10504498.

36. Hartner A, Marek I, Cordasic N, Haas C, Schocklmann H, Hulsmann-Volkert G, et al. Glomerular regeneration is delayed in nephritic alpha 8-integrin-deficient mice: contribution of alpha 8-integrin to the regulation of mesangial cell apoptosis. Am J Nephrol. 2008; 28:168–78. https://doi.org/10.1159/000110022 PMID: 17951999.

37. Hartner A, Cordasic N, Menendez-Castro C, Volkert G, Yabu JM, Kupraszewicz-Hutzler M, et al. Lack of {alpha}8-integrin aggravates podocyte injury in experimental diabetic nephropathy. Am J Physiol Renal Physiol. 2010; 299:F1151–7. https://doi.org/10.1152/ajprenal.00058.2010 PMID: 20826576.

38. Kriz W, Gretz N, Lemley KV. Progression of glomerular diseases: is the podocyte the culprit. Kidney Int. 1998; 54:687–97. https://doi.org/10.1046/j.1523-1755.1998.00044.x PMID: 9734594.

39. Hoffmann S. Angiotensin II Type 1 Receptor Overexpression in Podocytes Induces Glomerulosclerosis in Transgenic Rats. Journal of the American Society of Nephrology. 2004; 15:1475–87. https://doi.org/10.1097/01.asn.0000127988.42710.a7 PMID: 15153558

40. Nagata M, Kriz W. Glomerular damage after uninephrectomy in young rats. II. Mechanical stress on podocytes as a pathway to sclerosis. Kidney Int. 1992; 42:148–60. https://doi.org/10.1038/ki.1992.272 PMID: 1635344

41. Kriz W, Shirato I, Nagata M, LeHir M, Lemley KV. The podocyte's response to stress: the enigma of foot process effacement. Am J Physiol Renal Physiol. 2013; 304:F333–47. https://doi.org/10.1152/ajprenal.00478.2012 PMID: 23235479.

42. Kriz W, Lemley KV. A potential role for mechanical forces in the detachment of podocytes and the progression of CKD. J Am Soc Nephrol. 2015; 26:258–69. Epub 2014/07/24. https://doi.org/10.1681/ASN.2014030278 PMID: 25060060.

43. Hotchkiss Richard S., Strasser Andreas, McDunn Jonathan E., Swanson Paul E. Cell Death. The New England Journal of Medicine. 2009; 361:1570–83. https://doi.org/10.1056/NEJMra0901217 PMID: 19828534

44. Sato S, Yanagihara T, Ghazizadeh M, Ishizaki M, Adachi A, Sasaki Y, et al. Correlation of autophagy type in podocytes with histopathological diagnosis of IgA nephropathy. Pathobiology. 2009; 76:221–6. https://doi.org/10.1159/000228897 PMID: 19816081.

45. Hartleben B, Gödel M, Meyer-Schwesinger C, Liu S, Ulrich T, Köbler S, et al. Autophagy influences glomerular disease susceptibility and maintains podocyte homeostasis in aging mice. J Clin Invest. 2010; 120:1084–96. https://doi.org/10.1172/JCI39492 PMID: 20200449.

46. W Kriz. Maintenance and Breakdown of Glomerular Tuft Architecture. J Am Soc Nephrol. 2018; 29:1075–7. https://doi.org/10.1681/ASN.2018020200 PMID: 29535166.

47. Le Hir M, Keller C, Eschmann Valérie, Hähnel Brunhilde, et al. Podocyte Bridges between the Tuft and Bowman's Capsule: An Early Event in Experimental Crescentic Glomerulonephritis. Journal of the American Society of Nephrology. 2001:2060–71. https://doi.org/10.1681/ASN.V12102060 PMID: 11562404

48. Smeets B, Moeller MJ. Parietal epithelial cells and podocytes in glomerular diseases. Semin Nephrol. 2012; 32:357–67. https://doi.org/10.1016/j.semnephrol.2012.06.007 PMID: 22958490.

49. Grunewald TGP, Butt E. The LIM and SH3 domain protein family: structural proteins or signal transducers or both. Mol Cancer. 2008; 7:31. https://doi.org/10.1186/1476-4598-7-31 PMID: 18419822.

50. Lepa C, Möller-Kerutt A, Stölting M, Picciotto C, Eddy M-L, Butt E, et al. LIM and SH3 protein 1 (LASP-1): A novel link between the slit membrane and actin cytoskeleton dynamics in podocytes. FASEB J. 2020; 34:5453–64. Epub 2020/02/21. https://doi.org/10.1096/fj.201901443R PMID: 32086849.

51. Gagné V, Moreau J, Plourde M, Lapointe M, Lord M, Gagnon E, et al. Human angiomotin-like 1 associates with an angiomotin protein complex through its coiled-coil domain and induces the remodeling of the actin cytoskeleton. Cell Motil Cytoskeleton. 2009; 66:754–68. https://doi.org/10.1002/cm.20405 PMID: 19565639.

52. Hugo C, Nangaku M, Shankland SJ, Pichler R, Gordon K, Amieva MR, et al. The plasma membrane-actin linking protein, ezrin, is a glomerular epithelial cell marker in glomerulogenesis, in the adult kidney and in glomerular injury. Kidney Int. 1998; 54:1934–44. https://doi.org/10.1046/j.1523-1755.1998.00195.x PMID: 9853258

8. Eidesstattliche Erklärung

Hiermit erkläre ich, dass ich die vorliegende Dissertation selbständig verfasst und keine anderen als die angegebenen Hilfsmittel benutzt habe.

Die Dissertation ist bisher keiner anderen Fakultät, keiner anderen wissenschaftlichen Einrichtung vorgelegt worden.

Ich erkläre, dass ich bisher kein Promotionsverfahren erfolglos beendet habe und dass eine Aberkennung eines bereits erworbenen Doktorgrades nicht vorliegt.

Datum Unterschrift

9. Danksagung

Meiner Doktormutter Frau Prof. Dr. rer. nat. Nicole Endlich danke ich vielmals für das überlassen des Themas und das entgegengebrachte Vertrauen. Sie konnte mich im Gespräch für die experimentelle Arbeit in der Anatomie und Zellbiologie begeistern, dafür bin ich zutiefst dankbar. Darüber hinaus danke ich ihr für die Unterstützung und Freiheit bei der Durchführung, sowie die stete Erreichbarkeit und den angenehmen Umgang miteinander.

Ebenfalls danke ich Prof. Dr. med. Karlhans Endlich für die Leitung des Institutes in dem ich arbeiten durfte und für die zur Verfügung gestellten Mittel.

Besonderer Dank gilt Dr. rer. nat. Nadine Artelt für die tolle Betreuung und stetige Hilfe bei der Planung der Arbeit, Einarbeitung, Durchführung der Experimente sowie Auswertung. Herzlichen Dank für das offene Ohr, wenn Probleme oder Fehler auftraten, sowie die Hilfestellung zur Lösungsfindung; aber auch für die Unterstützung beim Verfassen des Papers. Weiterhin gilt ein großer Dank Dr. rer. nat. Felix Kliewe der meine Betreuung so kurzfristig übernommen hat und mir jederzeit mit Rat und Tat zur Seite stand und mich großartig während der Verfassung meines Manuskriptes unterstütze. Für die allumfassende Betreuung bin ich beiden zutiefst dankbar.

Den Kollegen der Arbeitsgruppe Endlich im Institut für Anatomie und Zellbiologie möchte ich vielmals für die stetige Hilfsbereitschaft danken. Mandy Weise danke ich besonders für die wertvolle Unterstützung bei Histologischen Färbungen, Sindy Schröder für die Hilfe bei den qRT-PCRs, sowie Claudia Weber für die Unterstützung und Beantwortung jeglicher Fragen. Weiterhin danke ich Dr. rer. nat. Antje Blumenthal für die große Hilfe bei der herausfordernden Elektronenmikroskopie. Herrn Jens van den Brandt und den Mitarbeitern der ZSFV danke ich für die Zucht und Bereitstellung der Mäuse. Dankbar bin ich Dr. Elke Hammer für die Analyse der Proteom Daten.

Einen großen Dank möchte ich auch an meine Freundin Kerrin Hansen aussprechen. Sie war eine unverzichtbare Ansprechpartnerin und Stütze während meiner Arbeit.

Der letzte und größte Dank gilt meiner Familie Carmen, Eric und Jana Ritter die mich in allen Lebenslagen bedingungslos unterstützen und auf die ich mich immer blind verlassen kann. In großer Dankbarkeit widme ich ihnen diese Arbeit.